AD NUMBER

AD484737

NEW LIMITATION CHANGE

TO

Approved for public release, distribution unlimited

FROM

Distribution authorized to U.S. Gov't. agencies and their contractors; Critical Technology; 28 JUN 1966. Other requests shall be referred to Air Force Rocket Propulsion Lab., Edwards AFB, CA.

AUTHORITY

AFRPL ltr, 20 Dec 1971

DOWNEY PLANT

RESEARCH DIVISION

PROJECT SOPHY

SOLID PROPELLANT HAZARDS PROGRAM

Technical Documentary Report No.
AFRPL-TR-66-25

Progress Report On
Contract AF 04(611)-10919

Report Number 0977-01(03)QP / June 1966 / Copy 134

AEROJET-GENERAL CORPORATION
Research Division
11711 Woodruff Avenue
Downey, California

PROGRESS REPORT

PROJECT SOPHY

SOLID PROPELLANT HAZARDS PROGRAM

Technical Documentary Report No.
AFRPL-TR-66-25

Contract AF 04(611)-10919

0977-01(03)QP

Period Covered: 1 March - 31 May 1966

R. B. Elwell
O. R. Irwin
Prepared by: R. W. Vail, Jr.

Date: 28 June 1966

Reviewed by: M. Nishibayashi
M. Nishibayashi, Head
Explosive Kinetics Dept

No. of Pages 86

Approved by: H. J. Fisher
H. J. Fisher, Manager
Research Division

Classification: UNCLASSIFIED

CONTENTS

ILLUSTRATIONS

ILLUSTRATIONS (Cont)

TABLES

1. INTRODUCTION

This quarterly progress report is the third of a series which partially fulfills Contract AF 04(611)-10919, Large Solid Propellant Boosters Explosive Hazards Study Program. The purpose of this program is to gain additional knowledge and to develop new techniques for analyzing the explosives hazard and damage potential of large solid-propellant rocket motors.

The objectives of this program are: (1) to determine the influence of grain shape on propellant detonability and sensitivity, (2) to determine the critical diameter of a typical solid composite rocket-motor propellant, (3) to determine what changes a solid-propellant grain might undergo when exposed to operational mishaps, and (4) to develop methods to simulate and characterize these alterations.

2. SUMMARY

- A critique of the RUBY computer code, as it is applied to detonation of solid propellant, has been prepared (see Appendix A).
- The detonation-model parameter c has been examined and analyzed further. Various hot-spot-producing phenomena in addition to porosity are considered.
- Critical-diameter test results for AAB-3189 indicate that the mean has shifted slightly from that computed with SOPHY I data.
- No pores between 12μ and 120μ diameter were detected following extensive microscopic examination of samples obtained from a charge cast from AAB-3225, despite the presence of a very large number of larger pores visible to X-rays.
- Critical-diameter tests of two batches of AAB-3225 show more than one inch difference in the computed critical diameters. A third batch has been requested.
- Detonation-velocity and reaction-zone-length measurements have been made on several supercritical samples of AAB-3189.

- Sustained detonation was observed in the large critical-diameter test (CD-96) involving a 6-ft-diameter sample of unadulterated propellant.

- The second and third large critical-diameter tests will utilize a 60-in. and an 84-in. diameter sample, respectively.

- Propellant defects, their synthesis and characterization, will be studied by Aerojet's Research and Technology Operations at the Sacramento Plant.

- Computer programs have been written to compute and print out graphically the following types of reduced data: detonation velocity vs distance down the charge, blast overpressure vs distance (including TNT curves for reference), impulse vs distance (also including TNT curves for reference), and fire-ball growth rate vs time.

3. THEORY OF CRITICAL GEOMETRY

3.1 THEORETICAL PROGRAM

3.1.1 Prediction of Ideal Detonation Properties

The RUBY computer code has been evaluated regarding its applicability to solid composite propellants. A series of compounds ranging from conventional high explosives to ammonium perchlorate, and formulations that included oxidizer plus aluminum or aluminum and binder, have been subjected to the RUBY program and the respective predictions analyzed. The evaluation process has included comparison with known experimental data, investigation of the trends that the principal parameters follow as functions of composition and density, and occasionally, comparison of the output with theoretically expected values.

The critique of RUBY, as an instrument for predicting the detonation parameters of composite propellant, is presented as Appendix A to this report. It is the conclusion of this analysis that the RUBY code is not applicable, in present form, to solid propellant. The principal disqualifying feature of RUBY is that the equation of state it uses is an unrealistic characterization of those conditions that are thought to apply in propellant detonation processes. Furthermore, RUBY is an empirical

tool, which must be adjusted internally by selection of the proper values of certain constants in the equation of state to agree in its predictions with experimental fact. It cannot be applied confidently to any compound or formulation that differs only slightly from the materials used to determine a particular set of its constants.

During the course of the evaluation of RUBY, considerable assistance has been given by individuals and organizations already experienced with RUBY and its operation. Among those to whom particular acknowledgement must be given are Dr. L. B. Seely of Stanford Research Institute, and J. Dieroff of the U. S. Naval Ordnance Test Station, China Lake.

3.1.2 Examination of the Parameter c in the Detonation Model

A mathematical model relating the critical diameter of an RDX-adulterated AP-composite propellant to the weight fraction of RDX has been previously developed (Reference 1). This model considers that the energy-release process within the detonation reaction zone is predominantly AP grain-burning, initiated at hot-spot sites provided by the rapid decomposition of the RDX particles. It is well established that porosity lowers the critical diameter of a material, presumably by providing a large number of hot-spot initiation sites at the shock-compressed pores. It was argued therefore that the small but finite concentration of internal flaws and pores unavoidably introduced into composite propellants during processing must be included with the RDX particles to obtain an estimate of the total hot-spot concentration which, through the model, determines the AP grain-burning time and the critical diameter of the propellant. In the SOPHY I model, the inherent hot spots are represented by an additional (constant) weight fraction c of RDX. The critical diameter d_c is then given by

$$d_c = k_1 \left(\frac{1}{f + c} \right)^{1/3} - k_2 \qquad (1)$$

where k_1 and k_2 are constants and f is the actual weight fraction of RDX.

Assuming a pore-size distribution in the propellant (Reference 2) and that such pores act as RDX particles of equal volume, the parameter c can be expressed in terms of the porosity, RDX content, and detonation-velocity, as follows (Reference 3):

$$c = \frac{1 - f}{1 + \frac{\rho_o \exp 3C_2/D^2 \,(1 - \rho_o/\rho_{o_n})}{\rho_R \left[(3C_2/D^2) + 1 - (\rho_o/\rho_{o_n}) \right]}} \qquad (2)$$

where ρ_o is the actual density of the propellant, D is the detonation velocity, C_2 is a constant, and ρ_{o_n}, the theoretical propellant density, is given by

$$\rho_{o_n} = \frac{1.756}{1 + 0.0633f} \qquad (3)$$

Using a value of 2.79×10^5 m^2/sec^2 for C_2 (Reference 2) and values of D from the graphical function of D_c vs f (Reference 1), values of c have been calculated for various assumed values of propellant density, ρ_o (and hence, porosity) The results are shown in Table 1.

Table 1. Estimation of c (ρ_o).*

Assumed Propellant Density, ρ_o (gm/cc)	Calculated Porosity (volume %)	Value of the Parameter c (as weight fraction RDX)
1.72	2.06	5×10^{-3}
1.73	1.49	1.6×10^{-3}
1.74	0.92	1.3×10^{-4}
1.75	0.36	5.1×10^{-9}

*Calculated for f = 0, and D = 3800 m/sec.

It is apparent that c will be quite sensitive to small changes in propellant density, so that holding c (and hence d_c) for unadulterated propellant within narrow limits will require extremely close control of (and ability to accurately measure) the density.

Based on the development in Reference 2, it can be shown that the number of effective pores per unit volume, N_p, is

$$N_p = \frac{1}{R_g^3} \exp\left[\frac{-3C_2}{D^2(1 - \rho_o/\rho_{o_n})}\right] \tag{4}$$

where R_g is the average AP grain radius.

The number of RDX particles per unit volume, N_R, is given by

$$N_R = \frac{3 f \rho_o}{4\pi \rho_R r_R^3} \tag{5}$$

where r_R is the average radius of the RDX particles. Also, the number of AP particles per unit volume, N_{AP}, is found from

$$N_{AP} = \frac{3(0.69 - f)\rho_o}{4\pi \rho_{AP} R_g^3} \tag{6}$$

Using a value of 2.79×10^5 m^2/sec for C_2, the measured value of propellant density for ρ_o, the theoretical propellant density ρ_{o_n} as given by Equation 3, and obtaining D from the graphical function of D_c vs f as given in Reference 1, the number of effective pores per 1000 AP particles ($N_\rho/1000N_{AP}$) and the number of RDX particles per 1000 AP particles ($N_R/1000N_{AP}$) have been calculated as functions of RDX content. The results are shown in Figure 1.

The minimum effective pore size can be found from the relation

$$r_i = \left(\frac{9C_2}{4\pi D^2}\right)^{1/3} R_g \tag{7}$$

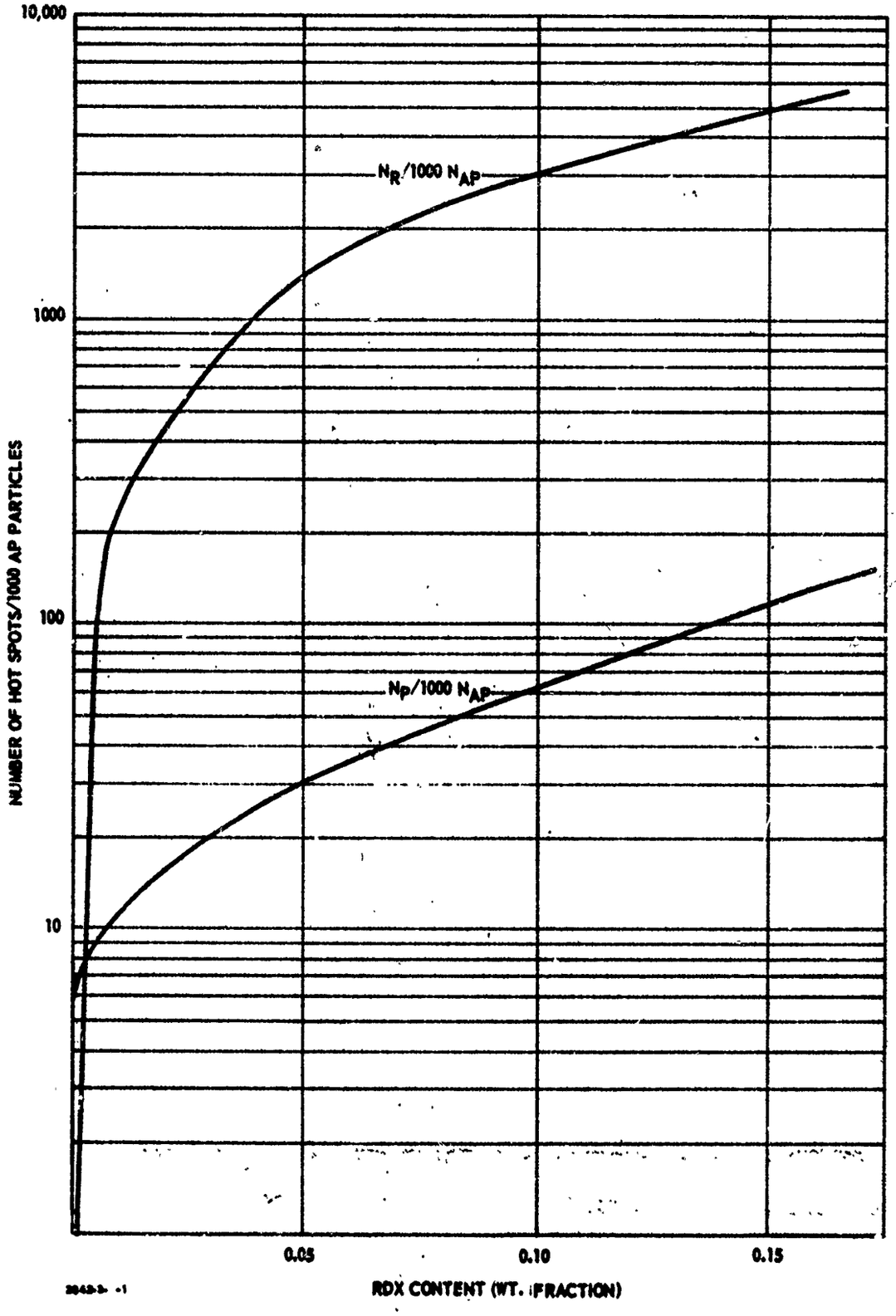

Figure 1. Hot-Spot Initiation Sites vs Content.

The calculated value of r_i varies from 4.8μ at f = 0.16 to 5.9μ at f = 0. The slight increase in the value of the minimum effective pore radius results from its dependence on D, which decreases from approximately 5000 m/sec at f = 0.16 to approximately 3800 m/sec at f = 0. (As the detonation velocity decreases, the minimum size or shock-compressed pore that is effective as a hot spot must be larger to contain the same minimum initiation energy.)

Although the probable presence of inherent porosity in composite propellants has been used as justification for introducing the parameter c, in reality c must include all hot-spot initiation sites, regardless of their origin. Available evidence indicates that many phenomena may lead to localized energy-rich regions (i.e., hot spots) when a shock wave passes through a material. Phenomena such as spallation, in which spalled material from the wall of a pore either decomposes during passage through the shock-heated gas in the pore or initiation reaction upon impact at the opposite surface of the pore (Reference 4), or Munroe jets (formed by appropriately-shaped pores) acting in the same manner as spalls (Reference 5) have been considered as alternatives to heating by adiabatic compression to explain the action of pores as hot spots. Shock reflection at interfaces between media of different impedances can also lead to an increased temperature. This mechanism may be an important one in providing "inherent" hot spots in the heterogenous AP-Al composite propellants by single or multiple shock-reflection at AP-Al interfaces of proper configuration. It has been recently proposed that some of the hot spots necessary for initiation may be produced by electrical breakdown of the crystals owing to a generated piezoelectric field (Reference 6). Refraction of shock waves around the inhomogeneities and subsequent convergence and interaction may also serve to produce "hot spots" downstream of the inhomogeneity (Reference 7).

Thus, although the parameter c was originally related to inherent pores in propellant, it will be equally applicable to any type of inherent hot spot source.

3.2 EXPERIMENTAL PROGRAM -- PHASE I

3.2.1 Variance and Mean Critical Geometry

To apply a statistical method to the reduction of critical geometry data, for the purpose of relating experimental results with theoretical predictions, it is essential that the variance as well as the mean critical dimensions be determined. There is a possibility that the variance is more a property of the material than of the particular shape under study. This subtask is designed to provide good estimates of the variance in critical geometry data obtained both from solid circular cylindrical charges and from solid square columnar charges. A comparison of the variances provides a first estimate of the geometrical effect on this quantity.

In the process of determining variance, the mean critical geometries of these two shapes necessarily are derived also. However, the specific design of the tests (the size-number distribution of the test articles) is that which serves best to determine the variance, rather than the mean.

The material used in these tests is AAB-3189 propellant, an RDX-adulterated ammonium perchlorate/PBAN propellant containing 9.2 weight percent RDX. Three 2000-pound batches of this material have been cast. The first two batches failed to meet project requirements. In the process of casting the first batch, 4EH-45, propellant viscosity exceeded castability limits before the operation was completed. The samples that had been cast were scrapped because of the suspect nature of the batch.

In the second try, batch 4EH-46, X-ray examination of the cured propellant grains revealed that a failure in the vacuum system had permitted an excessive number of air bubbles to be transported along with the propellant into the molds during the casting operation. The extreme porosity of these cured samples destroyed their value as test articles. The third batch was ordered immediately after discovering the condition of the second-batch samples. These events were responsible for delaying experimental work in this subtask by nearly two months.

The third batch, 4EH-85, was cast in early March, X-rayed on 28 March, and received in the Chino Hills Ordnance Research Laboratory in mid-April. X-ray examination of the articles disclosed small (less than 1/4-in. diameter) pores in 33 of the 50 samples. However, in most cases there were no more than two such pores in any one sample. Pore content of

this magnitude is not detrimental to critical geometry determinations. However, there were four samples that were rejected because they contained a hole or holes of 1/2-in. diameter or larger. Such discontinuities within the samples could interfere with sustained detonation, perhaps even to the point of quenching it.

3.2.1.1 Test Setup

The setup used in this subtask is the standard design that Aerojet has long employed in critical diameter testing. The test article is a solid cylinder (or a square column) of length equal to, or greater than, four diameters (or four times the length of a side). The explosive booster, of cast Composition-B explosive, is of similar geometry except that it is 3 diameters long. Each sample is weighed in air and in water to provide data by which its density is calculated. The assembled booster-acceptor stands on a 3/8-in.-thick mild-steel witness plate that is in turn elevated at least 1-in. above a base plate by two support blocks placed under opposite edges of the witness plate. Ionization probes are placed in the propellant to provide, via a rasteroscillograph, data from which velocity determinations are made.

The erect propellant charge with booster in place is measured at top, center, and bottom, and the dimensions recorded. From these measurements, a mean size is calculated, as well as the standard deviation, for each sample tested.

3.2.1.2 Data Accumulation and Reduction

Following the test, the witness plate is examined as a preliminary criterion of whether detonation was sustained. The probe-rasteroscillograph data are reduced by reading the time intervals between probe "blips" on the record. This information is supplied along with probe-spacing information as input to a computer, which is programmed to compute the velocity at each probe position (by numerical differentiation) and to print out the computed data in both tabular and graphical form. The data are presented as shock velocity vs distance down the charge. An example of such a plot is shown in Figure 2.

This computer program, along with others to be described at other places in this report, was written by Mr. D. G. Frutchey, of the Explosive Kinetics Department. These programs have contributed significantly to improvement in data reduction and presentation capabilities, with a substantially reduced cost.

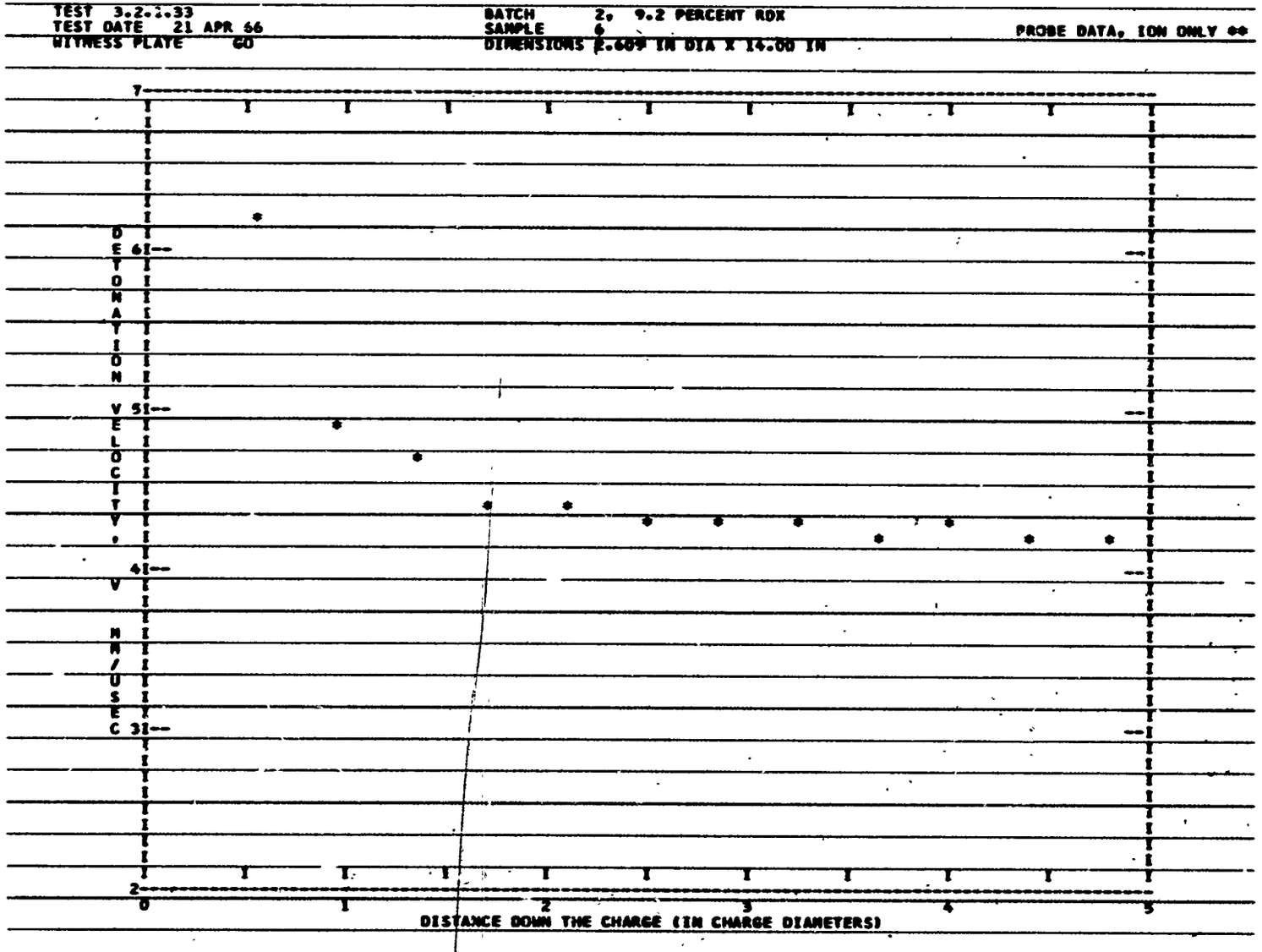

Figure 2. Detonation Velocity vs Distance, Test 3. 2. 1. 33.

3.2.1.3 Test Results

A summary of the results obtained from the 46 critical diameter tests is given in Table 2. The samples are listed in increasing order of diameter and, for those of the same mean diameter, in order of decreasing density. The go/no-go results from these tests are also shown in Figure 3. An attempt to obtain maximum-likelihood estimates of the mean (μ) and standard deviation (σ) was made using the computer program described in Reference 8, but the program would not converge to a maximum. For situations in which mixed results occur only at the lowest test level, the maximum-likelihood estimate of μ is the test level itself. The maximum-likelihood estimate of σ is zero. For such cases it is difficult to accept the maximum-likelihood estimates as being "best" estimates.

Better estimates might be those which the computer program uses as its first-guess estimates for the maximum-likelihood solution. These are obtained by combining the estimates derived by two other estimation techniques: the minimum overlapping subset method and the two subset method. Both of these methods and the method of combining them are described fully in Reference 8. From the data obtained in these tests, this estimating system calculates $\hat{\mu}$ = 2.59 in. and $\hat{\sigma}$ = 0.04 in.

3.2.1.4 Comparison with Previous Data

Since critical diameter data for AAB-3189 previously was generated, under Contract AF 04(611)-9945 (SOPHY I), it is natural to inquire how the two data sets compare, i.e., to determine whether the present data are compatible with the previous data.

Estimates made from the earlier set of data and from the combined data are shown in Table 3. A graph of the combined data is given in Figure 4.

A statistical test for whether the SOPHY I and SOPHY II data come from populations having the same cumulative normal response function can be made using the likelihood-ratio criteria. Defining

$$\lambda = \frac{L_o}{L_1 L_2} \tag{8}$$

where L_o is the maximized sample likelihood for the combined sets of data, and L_1 and L_2 are the maximized sample likelihoods for the individual sets, and restating Equation 8 logarithmically,

$$\ln \lambda = \ln L_o - \ln L_1 - \ln L_2 \tag{9}$$

Table 2. Test Results, Subtask 3.2.1.

Diameter		Density (gm/cc)	Results of Test	Average Detonation Velocity (mm/μsec)	Test No.
Mean (in.)	Standard Deviation (in.)				
2.60	0.006	1.726	Go	4.28	3.2.1.62
2.60	0.004	1.725	Go	4.28	3.2.1.40
2.60	0.003	1.723	No-Go	--	3.2.1.35
2.60	0.005	1.723	Go	4.25	3.2.1.37
2.60	0.005	1.722	Go	4.33	3.2.1.38
2.61	0.004	1.735	Go	4.26	3.2.1.61
2.61	0.001	1.729	No-Go	--	3.2.1.63
2.61	0.002	1.729	Go	4.26	3.2.1.64
2.61	0.003	1.728	Go	4.31	3.2.1.42
2.61	0.004	1.727	Go	4.25	3.2.1.60
2.61	0.003	1.724	Go	4.30	3.2.1.31
2.61	0.004	1.724	Go	4.25	3.2.1.36
2.61	0.005	1.724	Go	4.29	3.2.1.33
2.61	0.004	1.721	No-Go	--	3.2.1.32
2.61	0.005	1.721	No-Go	--	3.2.1.34
2.61	0.005	1.721	No-Go	--	3.2.1.29
2.66	0.025	1.725	Go	4.38	3.2.1.47
2.67	0.005	1.731	Go	4.33	3.2.1.52
2.67	0.007	1.729	Go	4.34	3.2.1.57
2.67	0.003	1.728	Go	4.32	3.2.1.55
2.70	0.004	1.725	Go	4.33	3.2.1.30
2.73	0.006	1.732	Go	4.37	3.2.1.56
2.73	0.012	1.723	Go	4.35	3.2.1.41
2.73	0.002	1.716	Go	4.36	3.2.1.46
2.74	0.003	1.729	Go	4.32	3.2.1.59
2.74	0.004	1.728	Go	4.37	3.2.1.58
2.78	0.002	1.738	Go	4.38	3.2.1.69
2.78	0.007	1.729	Go	4.41	3.2.1.68
2.78	0.005	1.723	Go	4.38	3.2.1.45
2.78	0.006	1.715	Go	4.36	3.2.1.28
2.79	0.006	1.735	Go	4.40	3.2.1.53
2.79	0.004	1.733	Go	4.44	3.2.1.71
2.79	0.003	1.729	Go	4.30	3.2.1.72

Table 2. (Continued).

Diameter		Density (gm/cc)	Results of Test	Average Detonation Velocity (mm/μsec)	Test No.
Mean (in.)	Standard Deviation (in.)				
2.79	0.004	1.728	Go	4.41	3.2.1.70
2.79	0.002	1.726	Go	(No Record)	3.2.1.44
2.79	0.005	1.721	Go	4.27	3.2.1.27
2.79	0.003	1.719	Go	4.39	3.2.1.67
2.79	0.005	1.719	Go	4.42	3.2.1.54
2.80	0.002	1.729	Go	4.41	3.2.1.51
2.80	0.002	1.727	Go	4.41	3.2.1.50
2.80	0.008	1.726	Go	4.38	3.2.1.43
2.80	0.003	1.720	Go	4.39	3.2.1.66
2.81	0.002	1.728	Go	4.38	3.2.1.48
2.81	0.006	1.724	Go	4.38	3.2.1.49

Average Density = 1.726 gm/cc

Standard Deviation = 0.0048 gm/cc

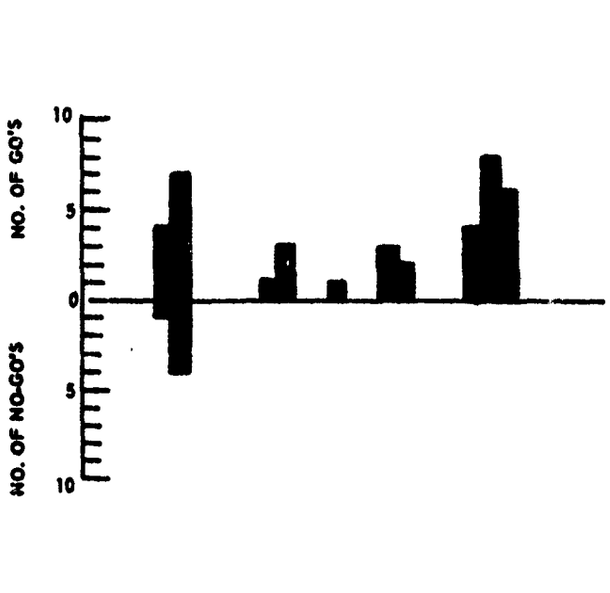

Figure 3. Critical Diameter Results, Subtask 3. 2. 1.

Table 3. Comparison of Critical-Diameter Estimates, AAB-3189.

Estimated Quantity	Symbol	AF 04(611)9945	AF 04(611)9945 in Combination with AF 04(611)10919
Mean (in)	μ	2.71	2.60
Standard Deviation (in)	σ	0.06	0.10
Covariance Terms	$\sigma_{\mu\mu}$	0.00053	0.00061
	$\sigma_{\mu\sigma}$	0.00001	-0.00039
	$\sigma_{\sigma\sigma}$	0.00052	0.00072
Ln Likelihood	lnL	-6.46	-25.05

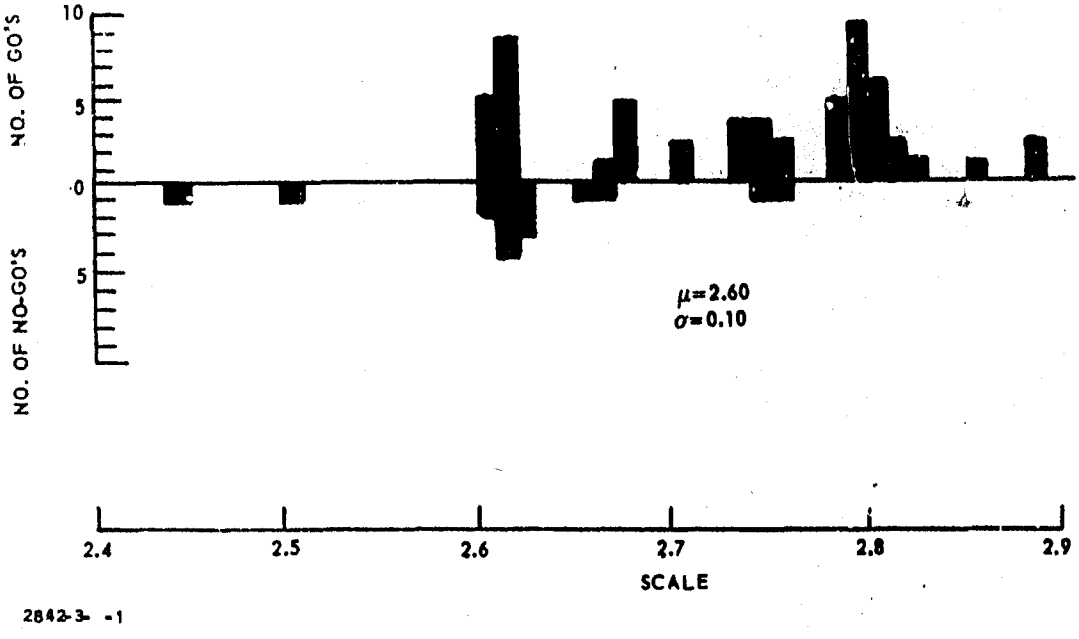

Figure 4. Combined Results SOPHY I and SOPHY II AAB-3189.

The quantity -2 ln λ approximately follows the chi-square distribution with, in this case, two degrees of freedom.

It should be remembered that the SOPHY II data did not yield a maximum-likelihood solution. Therefore, the application of the test to this situation must be considered approximate. If one assumes further that all of the SOPHY II mixed results occurred at one diameter, the sample log-likelihood for the SOPHY II data is (Reference 8):

$$\ln L_2 = 5 \ln 5 + 11 \ln 11 - 16 \ln 16 = 9.94 \qquad (10)$$

Substituting the sample log-likelihoods into Equation 8 gives

$$\ln \lambda = -8.65, \text{ or}$$

$$\chi^2 \leq 17.30 \qquad (11)$$

Since this large a value of chi-square is significant even at the 1% level, the test indicates that the two data samples do not come from populations having the same cumulative normal response functions.

Another method to compare the two sets of data consists of computing the joint confidence region for μ and σ for each set. If the computed ellipses do not overlap, it can be inferred that the samples come from different populations. If they do overlap, they could be from the same sample population. Evaluation of the joint confidence for μ and σ is given by determining those values that satisfy the equation

$$\left[\mu - \hat{\mu},\ \sigma - \hat{\sigma}\right] \Sigma^{-1} \begin{bmatrix} \mu - \hat{\mu} \\ \sigma - \hat{\sigma} \end{bmatrix} = \chi^2_{2,\,1-\alpha} \qquad (12)$$

where $\hat{\mu}$ and $\hat{\sigma}$ are the sample estimates, Σ is the covariance matrix of the estimates, and $\chi^2_{2,\,1-\alpha}$ is the value of chi-square with two degrees of freedom at the α significance level.

This will yield a (1 - α) confidence region. The values for Σ for SOPHY I data were shown in Table 3.

Since convergence to maximum-likelihood estimates was not achieved for SOPHY II data, corresponding estimates are not available. However, the covariance matrix for the SOPHY I data was used in conjunction with the μ and σ estimates for the SOPHY II data, and 95% confidence ellipses were calculated for each set. These are shown in Figure 5.

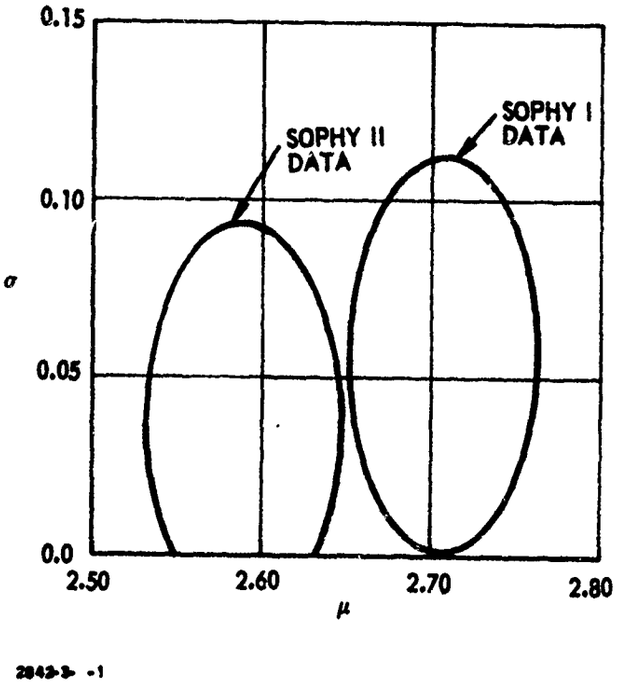

2842-3 -1

Figure 5. 95% Joint Confidence Ellipses for μ and σ, AAB-3189.

Although these ellipses do come quite close, they do not touch or overlap each other. Therefore, it is concluded from this test that the samples are from different populations.

The difference of the samples has been established by these two statistical tests, but the reasons for this difference must be learned. Several possible explanations exist. First, the ammonium perchlorate used in SOPHY II is from a different lot than that used in SOPHY I. Small, perhaps undetectable, differences between the lots may be responsible for the shift of the mean critical diameter by 0.12 in.

Second, the samples prepared for SOPHY II are being cast from larger batches produced on a different casting line, which introduces different size (and design) mixing equipment and different personnel. The shift to larger batches was an economic necessity that carried with it transfer of propellant casting from the research and development scale to the production scale. Such a move may account for the difference between the two sets of data.

Third, the difference could be explained by an uncontrolled material variability between batches. This possibility might be discounted, however, because of the close quality control requirements affecting ingredient acceptance and because of batch preparation controls.

Fourth, the statistical tests are only approximations to the actual situation; maximum-likelihood estimates for SOPHY II data were unobtainable and had to be artificially evaluated. Furthermore, the chi-square distribution at best is but an approximation to that of the log likelihood-ratio. The limitations on these methods of statistical analysis have been caused by the unfortunate fact that the standard deviation of the data for this material is very small, practically precluding the generation of mixed results at more than one size, plus the fact that the critical diameter was found to be at one end of the test range.

3.2.1.4 Future Plans

Another series of critical diameter tests will be conducted in July with samples cast in a batch that also will contain 50 square-column shapes. The results of the cylindrical tests will be compared with data from the two previous tests to determine whether these batch-to-batch differences in mean critical diameter are to be considered variations that are independent of batch size. Should these tests indicate that both SOPHY II sets can be from populations with the same cumulative normal response function, it will be assumed that for samples produced from one processing area, no significant batch-to-batch variation in critical geometry occurs.

3.2.2 Mean Critical Diameter and Variance

In this subtask the mean critical diameter of another RDX-adulterated AP-PBAN propellant (AAB-3225) was to be determined and an estimate of the variance of the data was to be calculated. The AAB-3225 formulation contained 7.1 weight-percent RDX and was expected to have a critical diameter of 6 in. The formulation will be used in later tests to determine the validity of the critical geometry theory as applied to a material different from AAB-3189, and for card-gap sensitivity tests for preliminary analysis of the relation between RDX-content and the initiation criterion for the two adulterated propellants. The estimate of variance will provide for a crude estimate of the variability of variance with critical diameter or with RDX content. It also will be required for statistical design of the verification tests, which will be conducted outside the mixed-result region for each shape.

3.2.2.1 Microscopic Analysis for Pores - Batch 4EH-44

Two batches of AAB-3225 have been cast and tested. Batch 4EH-44 produced data that were reported in the previous quarterly report (Reference 3). The samples had been X-rayed and the reports showed that, except for two samples, each contained approximately six major pores (less than 1/4-in. diameter) in its upper third with respect to casting position. When the critical diameter was found to be 5.21-in. instead of the expected 6-in., one of the very porous samples and one of the average samples were sent to Aerojet-Sacramento for microscopic analysis to determine whether the distribution of pores visible by X-ray inspection extended significantly down to the microscopic region (10 to 100μ sizes). If such small pores had existed in the propellant, the unexpectedly low critical diameter of Batch 4EH-44 material could have been understood as being the result of the increase in number of hot-spot initiation sites due to porosity.

The original large samples were prepared for the analysis by cutting them into disk-shaped sections, each of which was subsequently subsectioned. From the subsections, specimens were microtomed and mounted for microscopic examination. Each specimen was approximately 25 to 30μ thick, which placed a lower limit of 12 to 15μ on the pore sizes that could be observed. Figure 6 shows the sectioning plan used in these analyses.

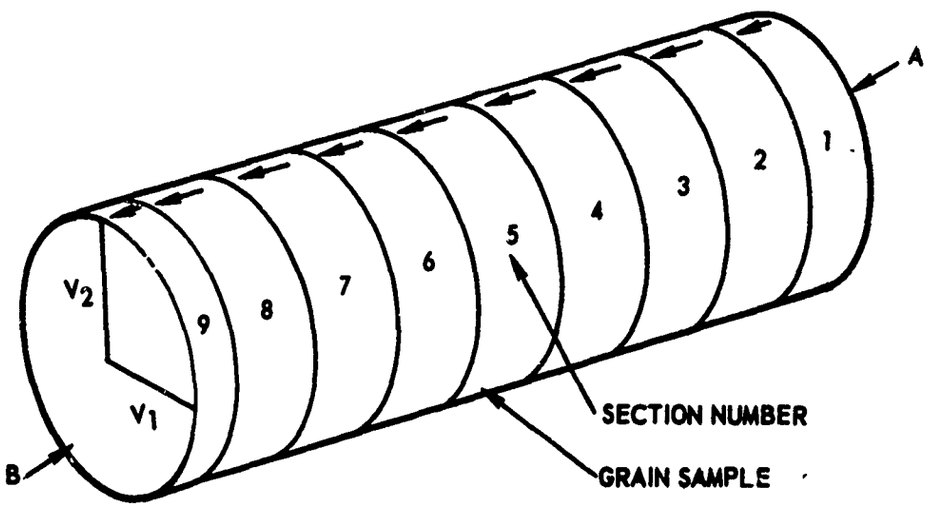

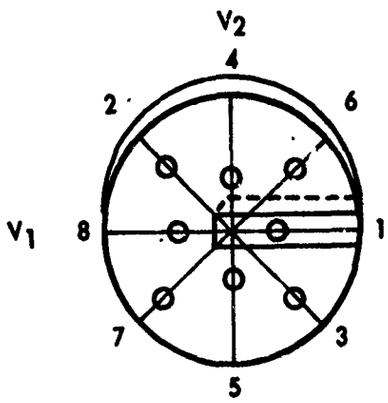

VIEW FROM END A

RADIAL SECTION PLAN
1-8 RAY INDEX NUMBER

O = PHOTOMICROGRAPH-MOSAIC LOCATION

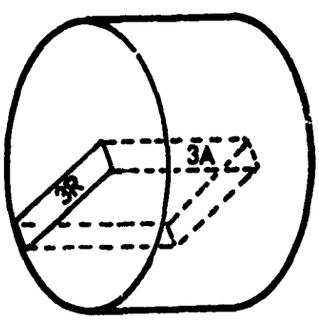

AXIAL SECTION PLAN
CODF NO. SECTION NO.
0.3 A AXIAL
0.3 R RADIAL

2842-2 -1

Figure 6. Sectioning Plan for Microscopic Analysis.

Photomicrographs were taken at 100X using a mechanical stage and a traversing technique that permitted the photos to be assembled into mosaics. Visual observation was performed at higher magnifications but because of the large number of photographs that would be required to map a significant area, no photographs were taken above 100X magnification. The photographs have been enlarged to double size.

No pores were discovered in the microscopic region for either sample. Representative photomicrographic mosaics are shown in Figures 7 and 8. In the photographs, the black areas are opaque aluminum particles, the large clear white areas are transparent ammonium perchlorate (AP) crystals, and the small (1mm) bright or gray spots are RDX crystals. The small voids within the AP crystals are common and must not be thought of as peculiar to the material used in this batch.

Re-evaluation of the predicted pore size that is effective as a hot-spot initiation site has led to the conclusion that pores of 2 to 5μ diameter can be effective. Their direct observation by microscopic techniques is beyond reach, however, because to prepare microtome specimens of the necessary thickness (4 to 10μ) and to permit their observation requires chipping a frozen propellant sample. Serious doubts can be raised as to the effect of such action on the physical condition of the sample. This fact, plus the extreme difficulty imposed by requiring a sample of uniform thickness, is further complicated by the fact that the surface area of such a thin specimen must be so small that the number of such specimens required to provide a representative sampling is unmanageably high.

3.2.2.2 Test Results - Batch 4EH-84

Batch 4EH-84 was cast to resolve the question of whether the previous data was obtained from acceptable material. The test design (sample sizes) was enlarged to cover both the range around the theoretically predicted critical diameter and the range tested with Batch 4EH-44. The test design and the test results are shown in Tables 4 and 5.

No overlapping of go and no-go results occurred, undoubtedly because of the large increment between diameters at that portion of the test design where the critical diameter was found.

No unique maximum-likelihood estimates of μ and σ can be defined. An estimate of μ would be given best by the midrange diameter between the largest diameter no-go and the smallest diameter go. For this set of data, $\mu = 6.36$ in. No estimate can be made of σ, but it apparently is not very large.

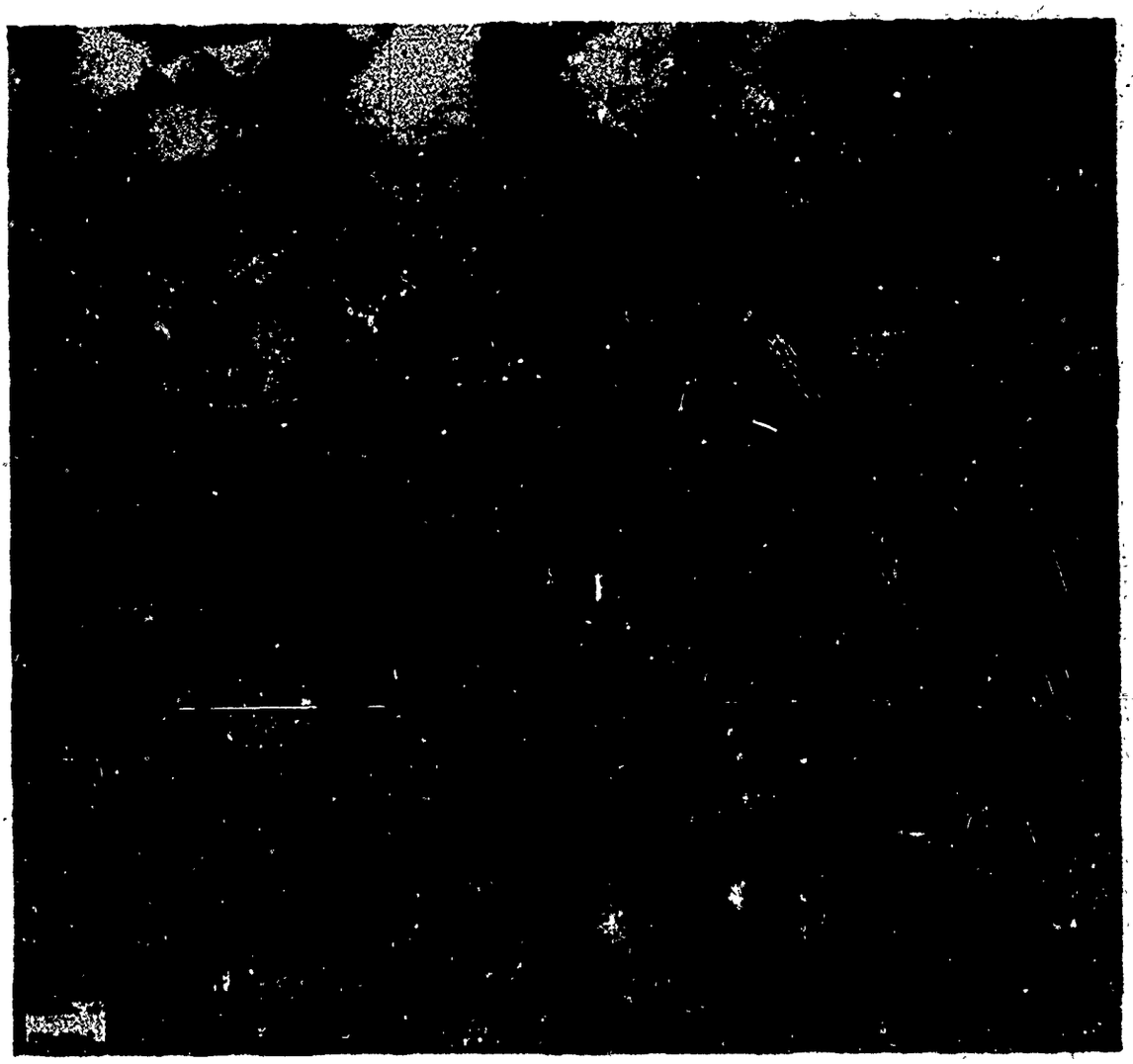

Figure 7. Photomicrograph of AAB-3225 Propellant Specimen 6A.

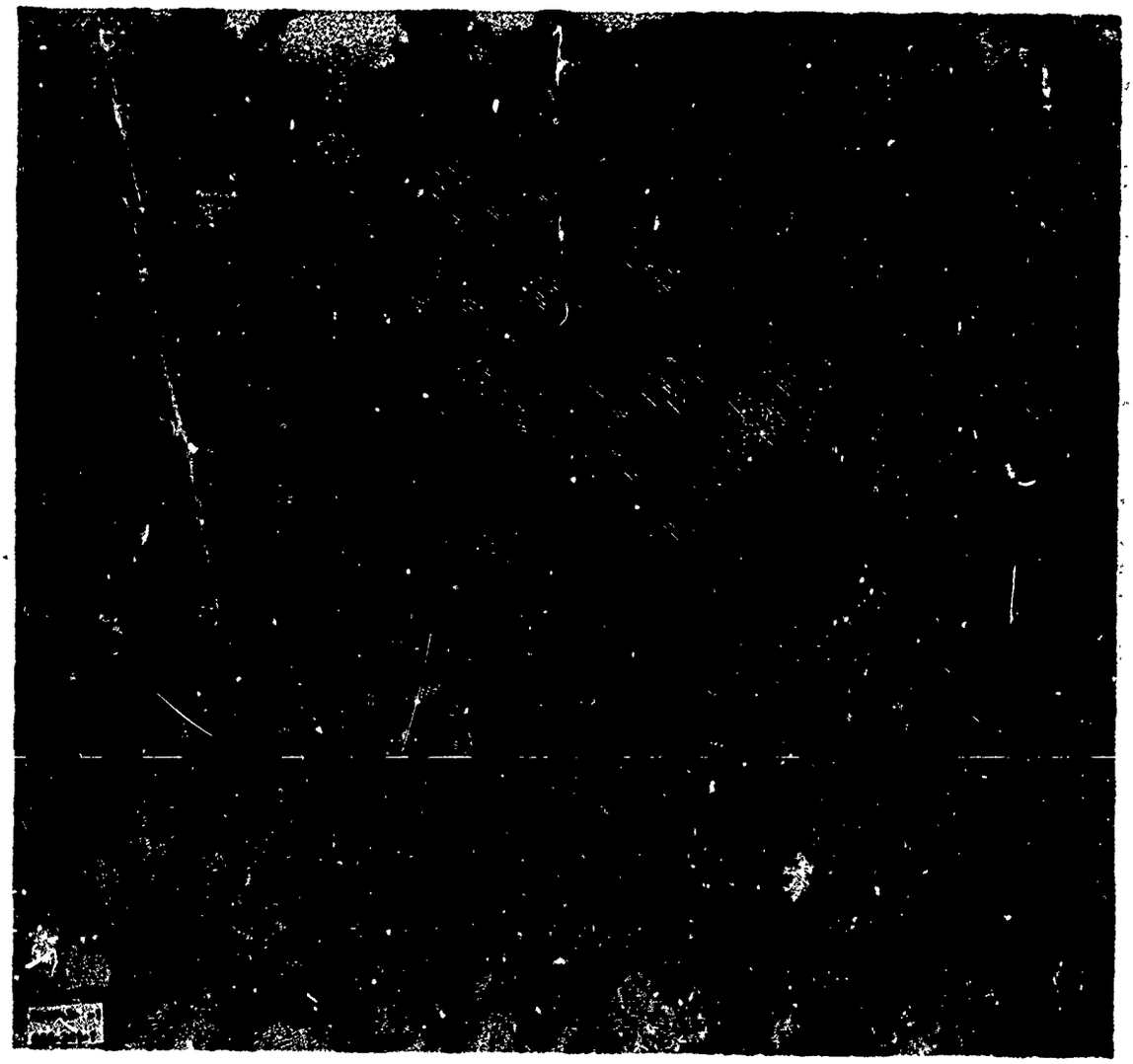

Figure 8. Photomicrograph of AAB-3225 Propellant, Specimen 2R.

Table 4. Test Design, Subtask 3.2.2 (Batch 4EH-84).

Diameter (in.)	No. of Samples
5.00	2
5.25	2
5.50	2
5.75	3
5.88	6
6.00	5
6.12	6
6.25	3
6.50	2
7.00	2

Table 5. Test Results, Subtask 3.2.2. (Batch 4EH-84).

Mean Diameter (in.)	Result (+ = go) (O = no-go)	Average Detonation Velocity (mm/μsec)	Test No.
5.49	O	--	3.2.2.38
5.49	O	--	3.2.2.39
5.98	O	--	3.2.2.40
5.99	O	--	3.2.2.41
6.09	O	--	3.2.2.51
6.09	O	--	3.2.2.52
6.10	-	--	3.2.2.43
6.10	O	--	3.2.2.50
6.23	O	--	3.2.2.46
6.24	O	--	3.2.2.44
6.48	+	4.25	3.2.2.45
6.48	+	4.15	3.2.2.47
6.97	+	4.33	3.2.2.42
7.00	+	Not reduced	3.2.2.48

The wide difference between the critical diameters of these two batches is extremely difficult to explain. The most plausible explanation is that the earlier batch was more porous. The second batch did not "slump" in the molds upon release of vacuum during the casting operation, while the slumping phenomenon did occur in the first batch during casting. The microscopic analysis does not support or reject the porosity hypothesis, because of the limited range of pore sizes that can be detected microscopically.

That this is the normal batch-to-batch variation to be expected for this formulation is intuitively impossible to accept. Compositional variation in RDX-content, for example, to account for such a shift in the critical diameter, is far beyond the tolerance limits allowed in the batch preparation and a major discrepancy of this type would appear in the batch preparation records. No such irregularity in composition has been detected following examination of all the batch records.

A third batch of AAB-3225 will be cast in June and tested in July to confirm or deny the apparent large batch-to-batch variability of the mean critical diameter.

3.2.3 Detonation Velocity as a Function of Size

This subtask investigates the relationship between detonation velocity, D, and size, d, from the near critical to the ideal geometry, for two shapes - the circular cylinder and the square column. Also to be determined is the relationship for these shapes between reaction-zone thickness a_0 and sample size. Such data is required to determine the validity of certain assumptions made in the detonation theory regarding the D(d, a) function (Reference 9). The material used in these tests is AAB-3189, which has a critical diameter of between 2.6- and 2.7-in. (Section 3.2.1). The diameters of the circular cylinders and the sides of the square columns to be tested are 4, 6, 8, and 12 in. The 12-in. size is more than four critical geometries large and the detonation velocity at this size is assumed to be sufficiently close to the ideal velocity to allow extrapolation to infinite diameter with reasonable confidence.

3.2.3.1 Detonation Velocity Measurements

The computed detonation velocities for 8-in.-diameter and 12-in.-diameter samples of AAB-3189 are shown in Table 6. The average velocity from three 12-in.-diameter samples is 4.76 mm/μsec; from seven 8-in.-diameter samples it is 4.70 m/μsec. From Subtask 3.2.1 data the average velocity obtained by considering all the velocities to be at 2.65-in. diameter (average) is 4.35 mm/μsec. These three points are shown on Figure 9 as D vs d, and Figure 10 as a D(1/d) plot which, when extrapolated to 1/d = 0, indicates that D_i (the ideal detonation velocity), is 4.88 mm/μsec. This velocity information is not complete, lacking data at 4- and 6-in.-diameters, so Figures 9 and 10 must be recognized as preliminary.

The three points do fit a first-order equation well within experimental error. The least-squares-determined equation for the line drawn in Figure 10 is

$$D = 4.875 - 1.391/d \qquad (13)$$

where D is given in mm/μsec, and d is given in inches.

Comparison of the average D's with those computed by Equation 13 is made in Table 7. Although the subtask has not been completed, and more data will be generated, the excellent linearity of the data is of value.

3.2.3.2 Reaction Zone Measurements

Measurement of reaction zone thickness is accomplished by using a conductive probe placed perpendicular to the axis of the sample. The shape of the pulse is generated in a sense by the shape of the reaction zone cross-section that is intercepted by the probe (Reference 3). Final reduction of the reaction zone shape data from the 8-in. and 12-in. diameter tests had not been completed. However, the shapes of the pulses differed from those generated in the preliminary tests, which used 4-in. diameter samples of detonable but unidentified propellant remaining from SOPHY I studies. The pulses produced by the 8- and 12-in. diameter samples are in trapezial shapes, rising rapidly to a peak amplitude, decaying linearly at a slow rate, and then dropping off rapidly to the original zero-level.

Table 6. Average Detonation Velocities for Supercritical 9.2% RDX Samples.

Diameter (in.)	Average Velocity (mm/μsec)	Test No.
12.0	4.74	3.2.3.1
	4.77	3.2.3.2
	4.77	3.2.3.3
8.0	4.70	3.2.3.4
	4.71	3.2.3.5
	4.71	3.2.3.6
	4.70	3.2.3.7
	4.67	3.2.3.8
	4.72	3.2.3.10
	4.69	3.2.3.11

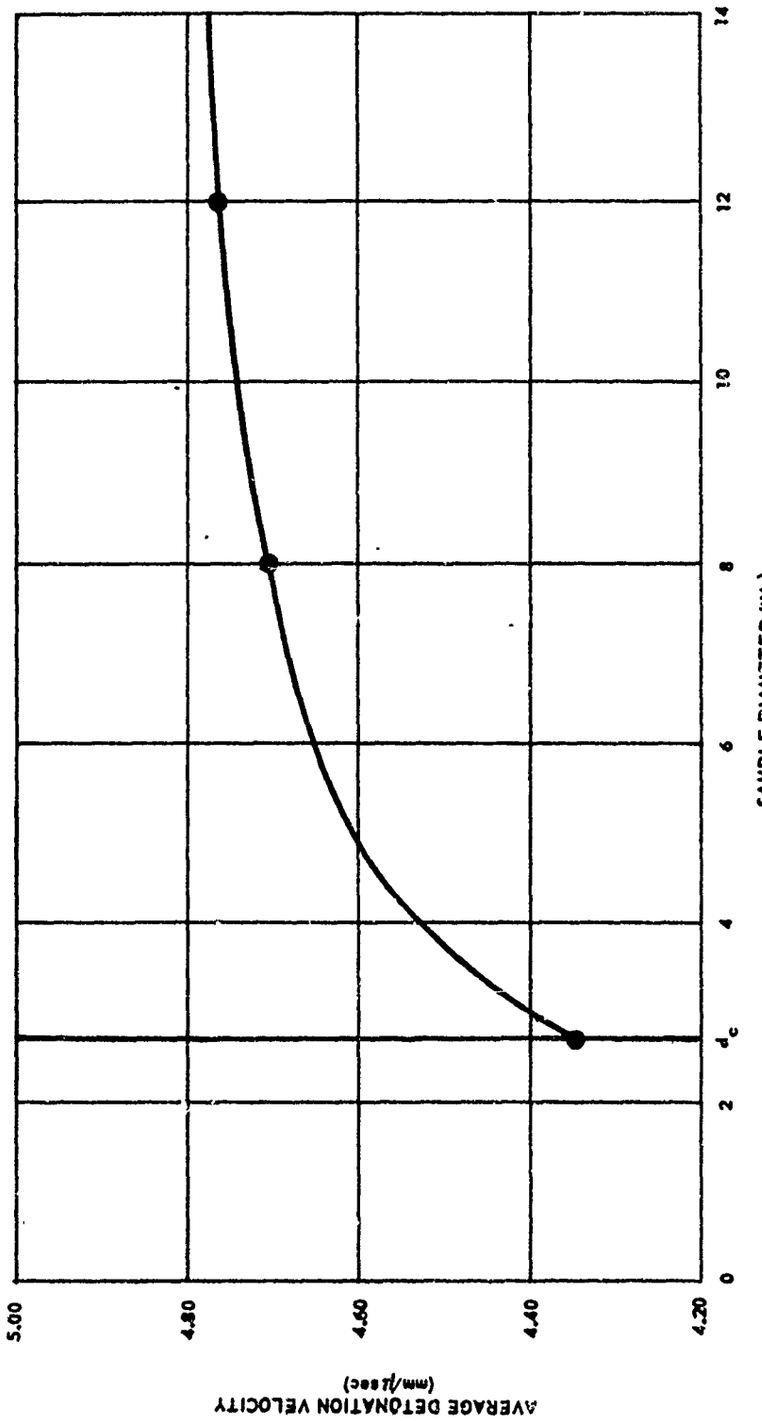

Figure 9. Detonation Velocity vs Diameter (AAB-3189).

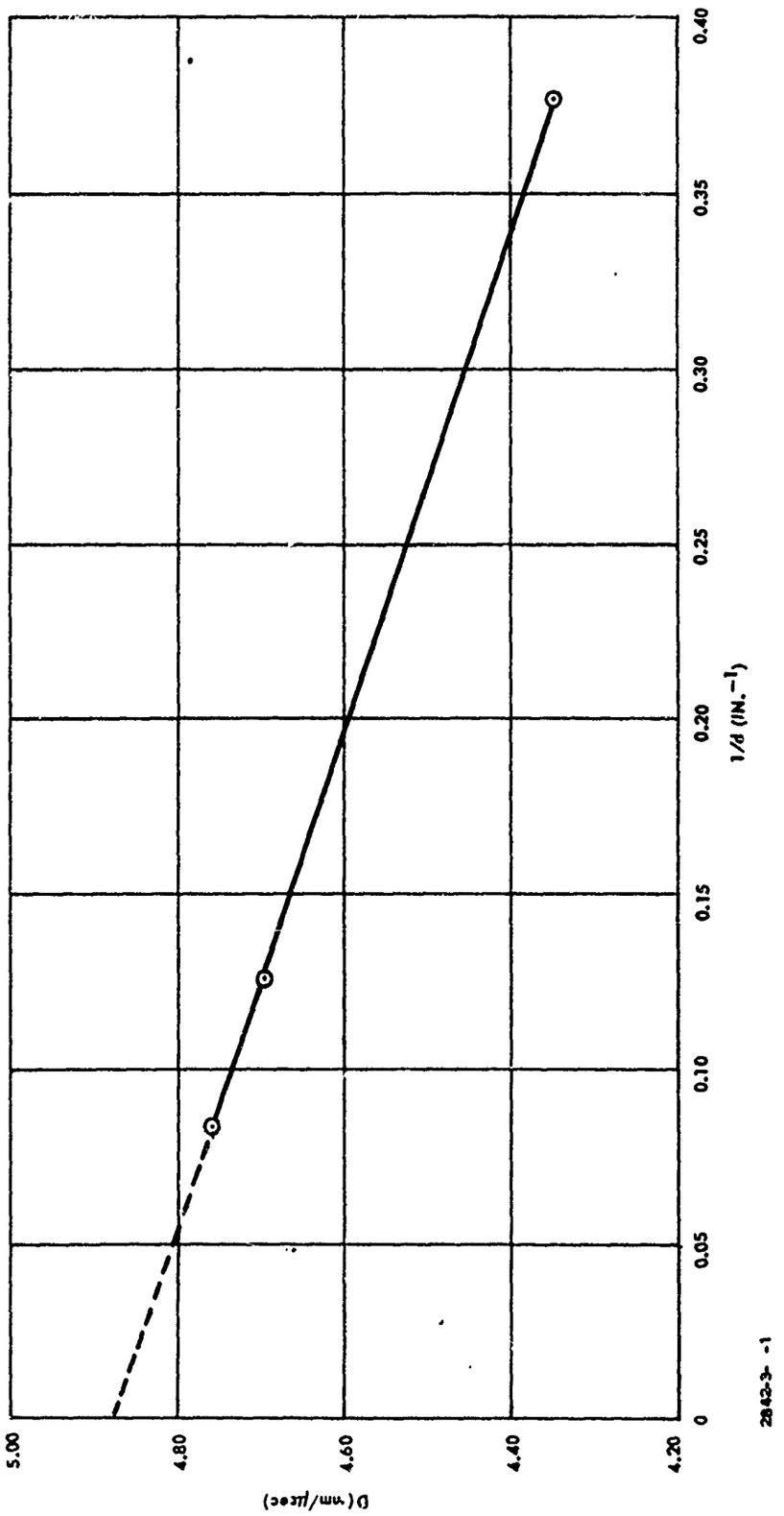

Figure 10. Detonation Velocity vs 1/Diameter (AAB-3189).

Table 7. Calculated vs Average Detonation Velocities (AAB-3189).

Diameter (in.)	Detonation Velocity	
	Average (mm/μsec)	Calculated from Equation 13 (mm/μsec)
2.65	4.35	4.350
8	4.70	4.701
12	4.76	4.759

Reaction zone shapes will be more difficult to infer from these pulses, however, because the signals are in most cases somewhat masked by external noise or transient pulses during the event. Efforts to increase the signal-to-noise (s-n) ratio have been moderately successful, but the samples used in these development tests were smaller sizes (about 6-in. diameter), which may have helped the s-n ratio.

The maximum (axial) reaction zone lengths have been determined from the pulse widths and the velocity data. The values of the reaction zone lengths for eight samples are given in Table 8. Two 12-in.-diameter samples were already tested before conductance probes were installed. Three more 12-in.-diameter samples will be cast soon to complete the original goal of four samples at each size. The first four 8-in. samples were from Batch 4EH-46; the last four tested were from Batch 4EH-85.

The reduced data for the 8-in.-diameter samples produce an average reaction zone length value of 6.3 in., with a standard deviation of 0.95 in. The accuracy of these data could be improved by using the exact detonation velocity past the probe instead of the average velocity in the sample region about the probe. Fluctuations of less than 2 percent observed in the detonation wave velocity as it proceeds through the lower half of the charge are not sufficient now to justify the use of more precise velocity data in making this determination.

3.2.4 Jetting Phenomenon Study

The purpose of this subtask is to study jetting, as it occurs in hollow-core cylindrical charges. The unusual results obtained during SOPHY I in the critical geometry determinations for hollow cylinders are believed to be the result of the occurrence of this phenomenon. In those tests (Reference 1) samples of sufficient web-thickness did sustain an apparent steady-state detonation, except that at some point down the charge the constant-velocity shock wave would abruptly attenuate. From one sample to the next, the distance down the charge that this point occurred increased as the web-thickness increased.

During the present effort the effect of core diameter on the detonative behavior of hollow cylinders will be studied. Also, a fixed geometry at various lengths, to learn more about the detonation of hollow-core cylinders, will be examined. The results of these investigations are needed to interpret the critical geometry concept as it relates to hollow shapes.

Molds have been designed and are presently being fabricated. Propellant casting is scheduled for June and testing will begin in July.

Table 8. Reaction-Zone Length Measurements
(Preliminary Data) AAB-3189.

Diameter (in.)	Detonation (mm/μsec)	Δt (μsec)*	a_o (cm)**	a_o (in.)**	Test No.
12	4.77	56	26.7	10.5	3.2.3.3
8	4.70	34	16.0	6.3	3.2.3.4
8	4.71	37	17.4	6.8	3.2.3.5
8	4.71	42	19.8	7.7	3.2.3.6
8	4.70	30	14.1	5.6	3.2.3.7
8	4.67	30	14.0	5.5	3.2.3.8
8	***	34	***	***	3.2.3.9
8	4.72	37	17.5	6.9	3.2.3.10
8	4.69	27	12.7	5.0	3.2.3.11

*Width of pulse, obtained using conductive probe.

**Reaction-zone thickness. Numerical values shown are calculated to one digit beyond the significant ones.

***No velocity data, hence no estimate of a_o. (Note that the duration time Δt is compatible with that of the other 8-in. diameter samples.)

3.3 EXPERIMENTAL PROGRAM -- PHASE II

With the authorization of the Air Force Contracting Officer received on 5 May 1966, Phase II, Task I, of Contract AF 04(611)-10919, has been initiated. Present efforts have consisted of designing molds and scheduling the mold fabrication, propellant preparation, and testing operations.

4. LARGE CRITICAL DIAMETER TESTS

Task II of this contract consists of analytical studies and large-scale testing to determine the critical diameter of a solid composite PBAN propellant, ANB-3226 This is the basic formulation from which the RDX-adulterated AAB-type propellants, used in SOPHY I and SOPHY II, are derived. Analysis of the SOPHY I data led to the choice of a 72-in.-diameter cylindrical grain for the first large test in the present program (Reference 10). The high cost of producing and testing such large-diameter propellant samples precludes the adoption of a conventional critical diameter test design to this task. It has been agreed that the greatest recovery of information would result from testing at three well chosen sizes rather than performing repeated tests at one diameter. In this sense, it is the precise objective of this task not to determine a mean critical diameter, but to determine the approximate critical diameter range and also to examine the subcritical and supercritical behavior of the unadulterated propellant (in terms of detonation velocity and blast and fireball characteristics).

Following the performance of the test of the 72-in.-diameter sample, the remaining two samples were selected as a 60 in. diameter and a 84 in. diameter. The 60-in.-diameter sample is midway between the 72-in.-diameter unadulterated propellant sample which detonated (see Section 4.1) and the 48-in.-diameter RDX-adulterated propellant sample that did not detonate when tested under Contract AF 04(611)-9945 (Reference 1). The latter contained 0.25 weight percent RDX. The implication of the no-go results is that a 48-in.-diameter unadulterated propellant sample also would be subcritical. The result of the planned 60-in.-diameter test will narrow the go/no-go region to half its present size. If this test is positive (a go), the critical diameter may be assumed to be 4 to 5 ft; if it is negative, the critical diameter may be assumed to be 5 to 6 ft.

The 84-in.-diameter sample will be tested to acquire data of extreme value to the understanding of the behavior of solid composite propellant in the supercritical regime. This will benefit both the theoretician and the engineer, for it will provide information regarding detonation velocity and blast and fireball characteristics of composite propellant at a level heretofore never tested. The detonation-velocity measurement will furnish a second (or third, if the 60-in.-diameter sample detonates) point in a detonation-velocity-vs-diameter function and thereby reveal whether this function behaves similarly to that which has been deduced from high-explosive studies. The sizes of existing and anticipated large-solid boosters make the blast and fireball data from the 84-in. test particularly invaluable, since it is apparent that these boosters may well be of supercritical dimensions.

4.1 TEST CD-96, (72-IN. DIAMETER)

The largest critical diameter test yet performed was conducted in Area 1-36D at the Air Force Rocket Propulsion Laboratory (AFRPL), Edwards, California, on 29 March 1966. A 6-ft-diameter solid cylindrical sample of ANB-3226 propellant (ammonium perchlorate oxidizer and aluminized polybutadiene-acrylic acid-acrylonitrile binder) sustained steady-state detonation over the lower 2-1/2 diameters of its original 4-diameter length. The detonation velocity was approximately 3.2 mm/μsec, measured by ionization probes with a rasteroscillograph system.

4.1.1 Test Setup

The propellant acceptor charge was constructed at the test site from five 6-ft-diameter by 4.8-ft-high segments of ANB-3226 propellant. Each segment contained more than 7 tons of propellant; the total propellant weight was approximately 37 tons. The segments were shipped in their molds from Aerojet's Solid Rocket Operations Plant at Sacramento. At the test site, each mold was removed and an 0.080-in.-thick aluminum cylindrical restraining fixture was fastened around the bare propellant.

The excessive loading experienced by the propellant in its final test position required the application of a restraining fixture to preserve dimensional uniformity and physical integrity. The aluminum "girdle" design represented the minimum confinement consistent with meeting the stress loads that were anticipated.

The girdles provided sites from which tie-down cables were attached to secure the segments in a three-point pattern to "deadmen" buried 40 ft from the charge. The segments were positioned and tied down to form an exactly vertical column, determined by triangulation with a pair of transits.

The propellant segments were lifted into their final positions by a vacuum chuck assembly capable of handling propellant in diameters up to 96 in. Woven straps beneath the segments provided physical support against a vacuum failure. Each segment-lifting operation proceeded without event, proving out the vacuum chuck design.

The TNT booster consisted of stacked segments, each measuring 3-ft thick. The shape of each segment resembled three 1-ft-thick cylindrical sections, whose diameters decreased by 4 in. progressing toward the top of the segment. Thus, a 3-to-1 height-to-base-diameter cone was approximated.

The estimated weight of the booster was 18,000 lb. The booster molds, in and by which the segments were lifted, were removed after each segment was finally positioned. Tie-down cables were attached to rings placed at two levels on the booster to secure the TNT.

This configuration was 42 ft high. The detonator was placed in a final cone of C-4 explosive placed on top of the stacked TNT booster.

The test setup is shown schematically in Figure 11. The leveled test pad consisted of a square concrete ring measuring 10 ft on a side. The individual sides of the ring were 1 ft wide at the top, 21 in. wide at the bottom, and 4 ft deep buried in the soil. The soil inside the ring was removed to a depth of approximately 8 in. to provide the customary air gap beneath that portion of the steel witness plate under the charge.

The need for this support arrangement was dictated by the questionable ability of the soil, at ground zero, to provide stable support for wood beams under the plate. Because of the refilling of craters left after each 48-in.-diameter test on Contract AF 04(611)-9945, it was estimated that the ground was not strong enough to support the 60-ton load imposed by the witness plate, propellant, and booster.

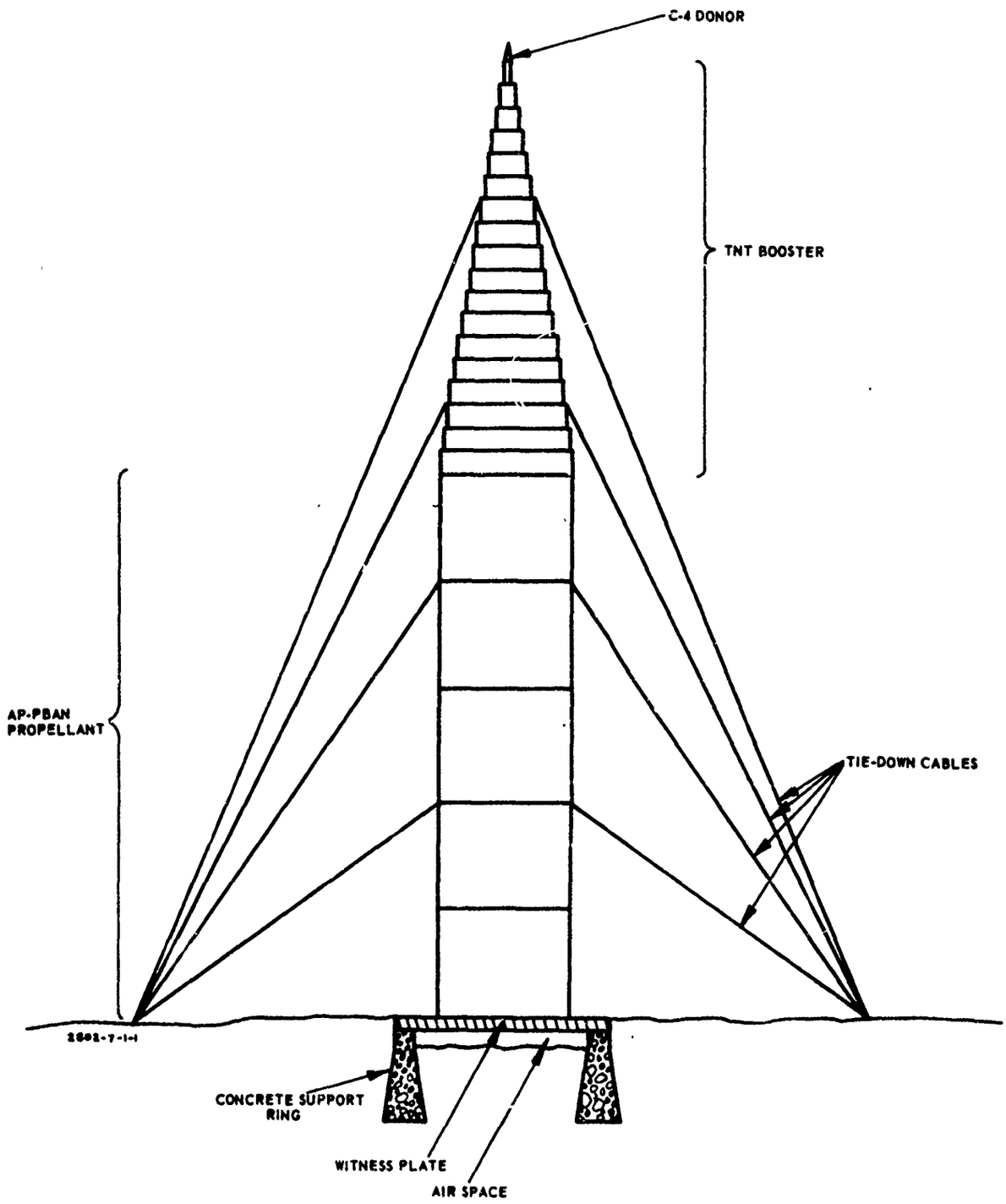

Figure 11. Critical-Diameter Test Setup for 72-in.-Diameter Sample.

The witness plate was a mild-steel plate, 6 in. thick by 10 ft square, weighing approximately 12 tons. The handling of this plate was facilitated by ear lugs welded at its edges. A 45-ton-capacity crane provided by the Air Force was used to lift the plate and the propellant and booster segments. Figure 12 shows the complete test configuration standing on the witness plate, at the moment when the ionization probes were being inserted and checked out. The uppermost segment of the booster assembly (see Figure 12), available from the SOPHY I project, was not designed to be removed from its mold; consequently, this configuration had plywood strengthening rings and an aluminum sheet around that segment.

4.1.2 Instrumentation

4.1.2.1 Detonation-Velocity Measurement

Ionization probes of two designs were used with rasteroscillograph systems to provide detonation-velocity data. These probes were placed along the length of the propellant sample in two rows, one for each type of probe, located 90 degrees apart on the charge surface. Holes in the restraining girdles provided access to the propellant surface at the locations selected as probe sites.

To provide a streak record of the event, a modified Beckman and Whitley Model 318B camera with 35mm film was synchronized with the firing of the charge.

The low level of luminosity from detonating adulterated propellant, which is also expected to be characteristic of unadulterated propellant, plus the distance the camera had to be placed from ground zero, put a heavy demand upon the lens system of the camera. The camera employed in this test includes a 629mm objective lens.

4.1.2.2 Blast Overpressure and Impulse Measurement

A Kistler system provided side-on and face-on blast pressure data. This system consists of Type 601A and 701A side-on gauges, Type 601A face-on gauges, and Kistler amplifiers. The output from the system was recorded directly on FM tape, using Ampex FR1200 (120 ips) and Ampex ES100 (60 ips) recorders. Location of the instrumentation legs is shown in Figure 13.

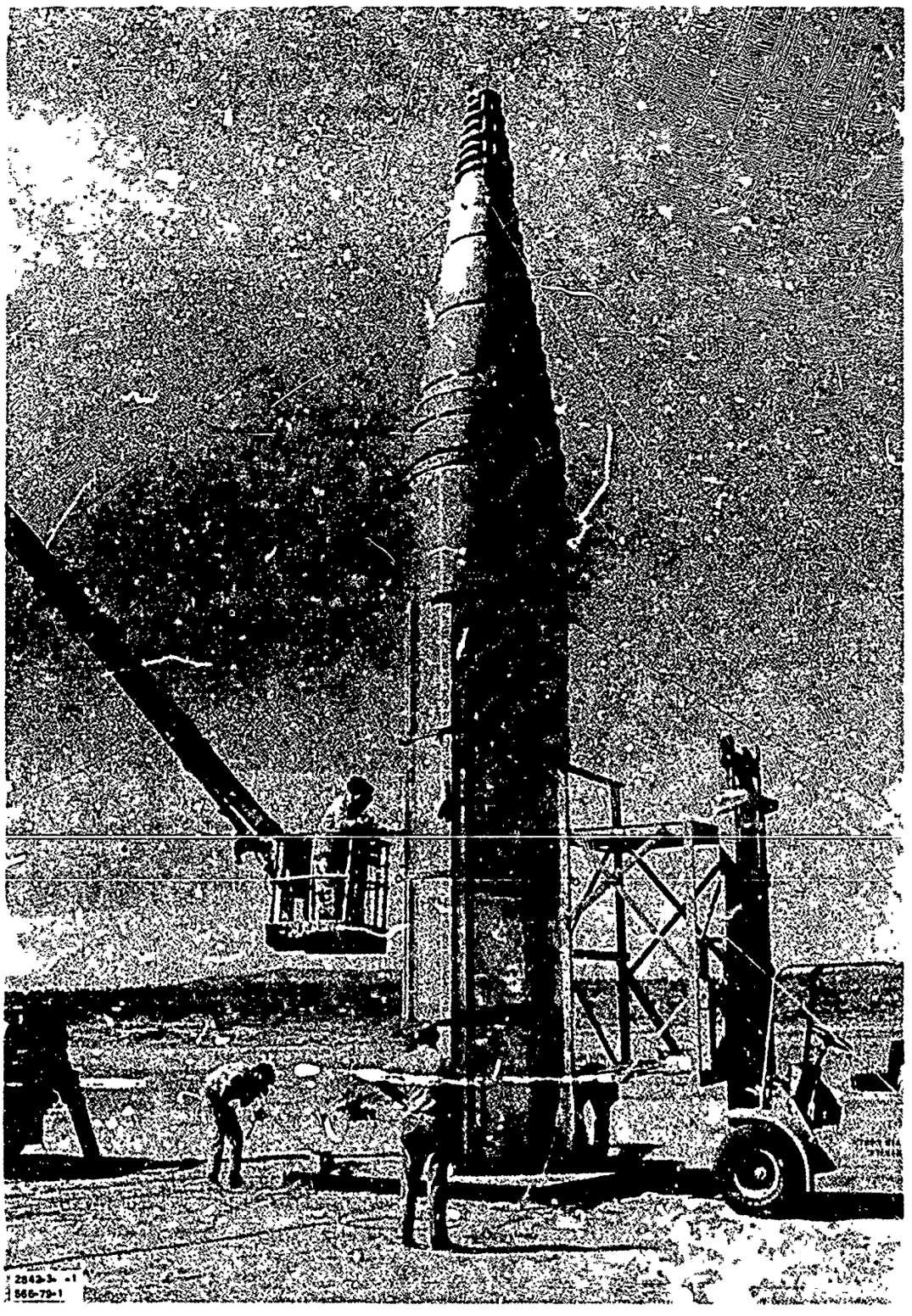

Figure 12. 72-in. Critical-Diameter Test Setup CD-96.

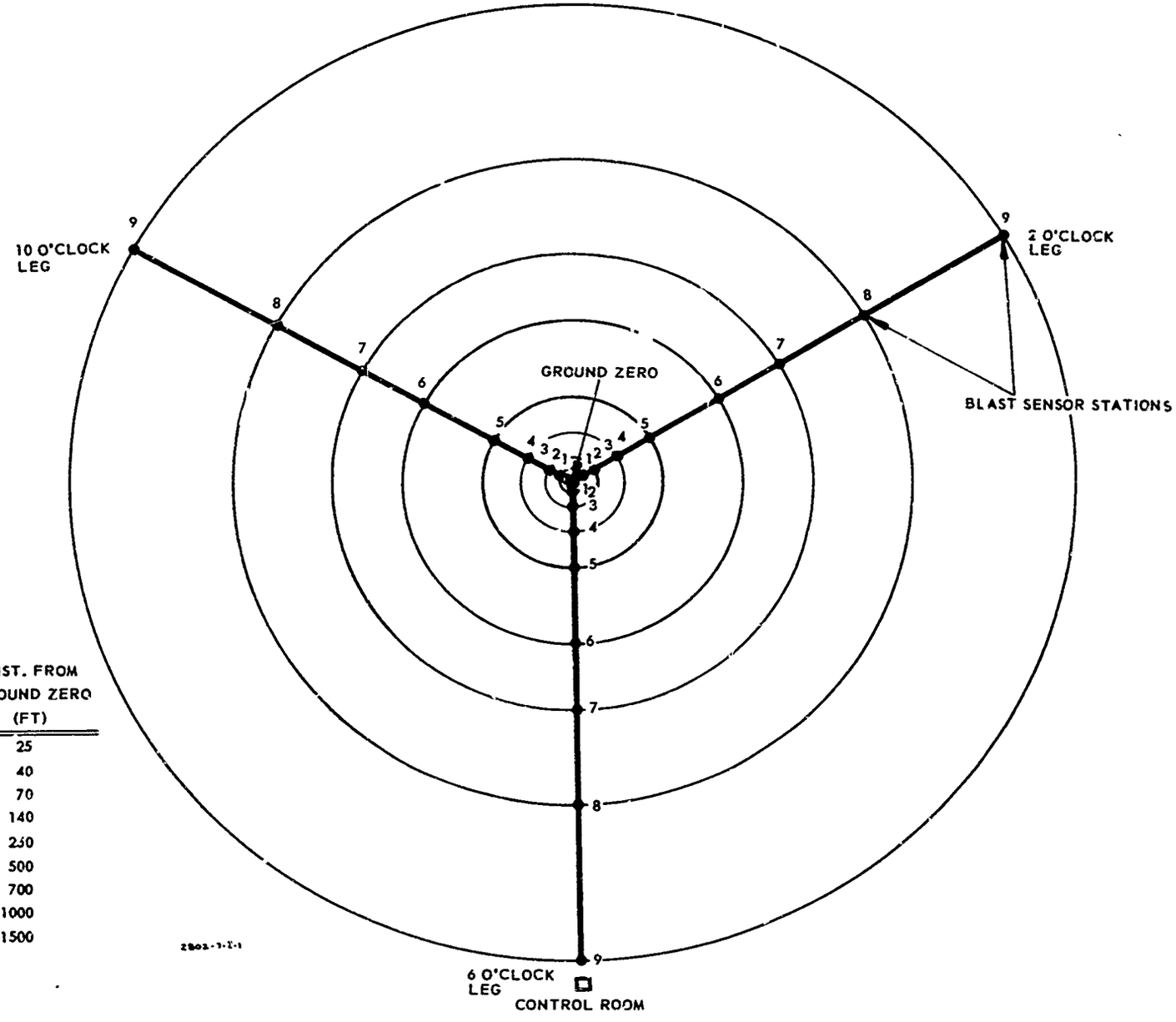

STATION NO.	DIST. FROM GROUND ZERO (FT)
1	25
2	40
3	70
4	140
5	250
6	500
7	700
8	1000
9	1500

Figure 13. Blast Instrumentation Legs, AFRPL 1-36D Facility.

An integrating circuit has been devised and checked out to automatically integrate the overpressure-time curves direct from the tape recorder during playback. This system will reduce data reduction time when it replaces the manually operated planimeter method.

Another significant development in Aerojet data reduction capabilities is a computer program which is being perfected that will accept peak overpressure and impulse data and perform calculations to present the data graphically vs distance. On the graphs will appear corresponding curves for 50, 100, and 200 percent TNT. This format will facilitate interpretation of the data.

4.1.2.3 Fireball Growth Rate

Documentary and high-speed photographic coverage of the firing test was provided by five Fastax cameras, two Milliken cameras, and a 35mm camera. The Fastax and Milliken cameras were operated at film speeds ranging from 64 fps to 8000 fps and the 35mm camera at 6 fps. Helicopter-borne cameras recorded the event on 70mm film at 20 fps and 16mm film at 200 fps. Except for the black-and-white 70mm film, all the film used was color.

The principal purpose of this camera coverage is to provide records from which the fireball growth rate can be calculated. In addition, the coverage makes it possible to measure the wave velocity along the ground independently of the blast gauges. It also provides a means of detecting the emergence of burning propellant fragments from the fireball; such fragments are characteristic of nondetonating propellant charges.

4.1.2.4 Fireball Radiation

Instrumentation placed within the expected 700-ft-radius fireball region to measure fireball heat flux and radiation included two pairs of Deltacouples and two radiometers. These were located in two stations, each consisting of a Deltacouple pair and a radiometer. In addition, the instrumentation included a pyrometer to measure the fireball temperature.

4.1.2.5 Audio Level

As part of the instrumentation designed for this test, it was decided to include a sound-level record at the 1/2-psi overpressure level. Assuming 100 percent TNT equivalence for the propellant, the gauge site was determined to be 3400 ft from ground zero. The system employed was a B&K Instruments No. 2203 sound-level meter with a No. 4133 1/2-in. microphone.

4.1.3 Test Results

4.1.3.1 General Observations

Eyewitness observation of the test, and subsequent examination of the photographic records, revealed that no burning propellant was expelled in the test. Furthermore, a nearly hemispherical air shock is clearly visible in more than one film record. Based on these observations, no evidence of a no-go can be found in the photographic records. The event as recorded by a 35mm camera at 6 fps is shown in Figures 14 and 15.

Fragments of the aluminum restraining fixtures used in CD-96 were collected after considerable searching of the area. All the recovered fragments are shown in Figure 16. The size and condition of these fragments offer further evidence for the detonation of this propellant. These are the only fragments that have been sighted.

The witness plate was severely broken up by the detonation. In all previous no-go's in the large critical-diameter tests on Contract AF 04(611)-9945, the witness plates were dished but not broken. In all previous go's, the plates were punched and strong evidence of flow was observed at the portions of the plates beneath the periphery of the charges.

The witness plate fragments from the 72-in.-diameter test have not shown the characteristic flow. However, the velocity data (see Section 4.1.3.2) provide the most probable answer to this problem. The calculated shock pressure corresponding to a detonation velocity of approximately 3.2 mm/μsec in this propellant in 45 kbar. Transmitted to steel, this pressure would not exceed 90 kbar. Yet NOL data (Reference 11) indicate that 95 kbar is required to punch a 3/8-in.-thick, mild-steel plate. Therefore, it may be concluded that the witness plate reaction to the low-velocity detonation produces results different from

FRAME 1

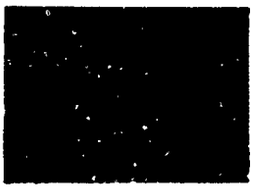

FRAME 2

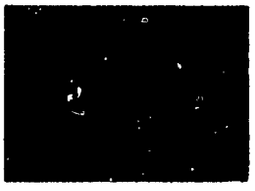

FRAME 3

FRAME 4

FRAME 5

2842-3-14-1

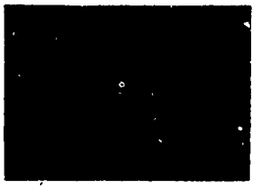

FRAME 6

Figure 14. Test CD-96, Photographed at 6 fps, Frames 1-6.

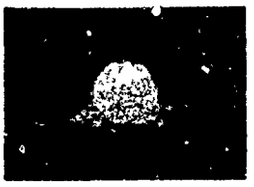

FRAME 7

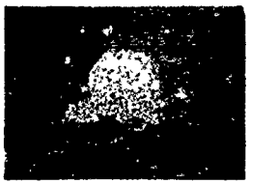

FRAME 8

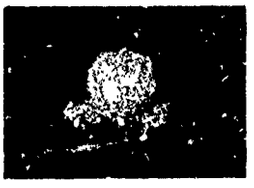

FRAME 9

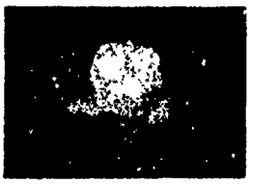

FRAME 10

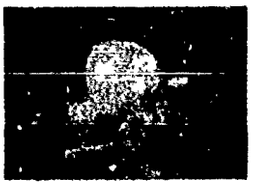

FRAME 11

FRAME 12

2842-3-15-1

Figure 15. Test CD-96, Photographed at 6 fps, Frames 7-12.

Figure 16. Fragments of Aluminum Sheet from Test CD-96.

those generally observed with high-velocity detonations. Concerning the witness-plate technique, the presence of a characteristic punch is ample evidence of a go, but the absence of such a reaction is not sufficient proof of a no-go.

The crater left by the shot measured 32 ft in diameter and 10 ft deep (to the backfill level). Figure 17 is a photograph of the crater, showing the largest piece of broken witness plate in the foreground.

4.1.3.2 Detonation Velocity

The probe-rasteroscillograph systems produced excellent records of a sustained detonation over the lower 2-1/2 diameters of the charge. The average detonation velocity from these probe records is 3.2 mm/μsec. Sonic velocity in this propellant is estimated at 1.9 mm/μsec. The observed velocity is clearly supersonic and steady-state. From these data there can be no doubt that the sample did detonate. Figure 18 shows the plotted values of detonation velocity vs distance down the charge. The split-probe data were generated from an experimental probe design being evaluated in the test. While not accurate, perhaps because of nonuniform fabrication, these probes did provide nominal support to the ion-probe data and for that reason their data are shown. The streak record for CD-96 was lost because of a failure by the film cassette to properly engage the film for removal from the camera. As the result of this failure, the entire film length was exposed to daylight.

4.1.3.3 Blast Overpressure and Impulse

The records obtained from the Kistler blast gauges have been read for peak overpressure and impulse at the various gauge stations. Reproductions of the actual profiles are presented in Figure 19 through 24 to show the generally excellent quality of the raw data. In each figure the calibration step represents the overpressure level that is indicated by the adjacent numerical value, and the overpressure-time profile is shown at the right. The calibration steps are generated artifically by applying a certain voltage to the system. They are evaluated in psi by knowing the transducer sensitivity (pico-coulombs per psi) and the amplifier gain-setting.

Figure 17. Crater, Test CD-96.

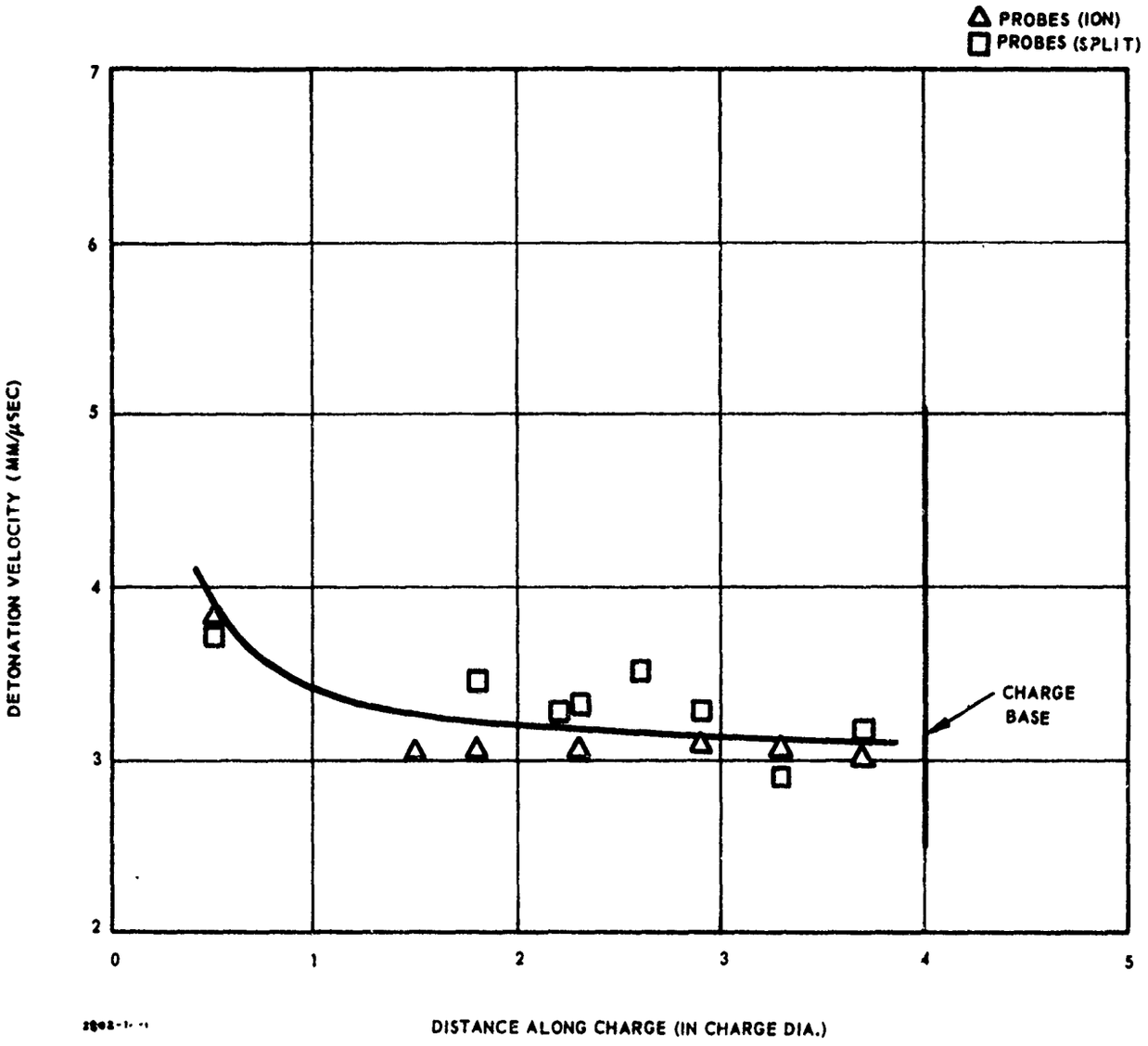

Figure 18. Detonation Velocity vs Distance Along Charge.

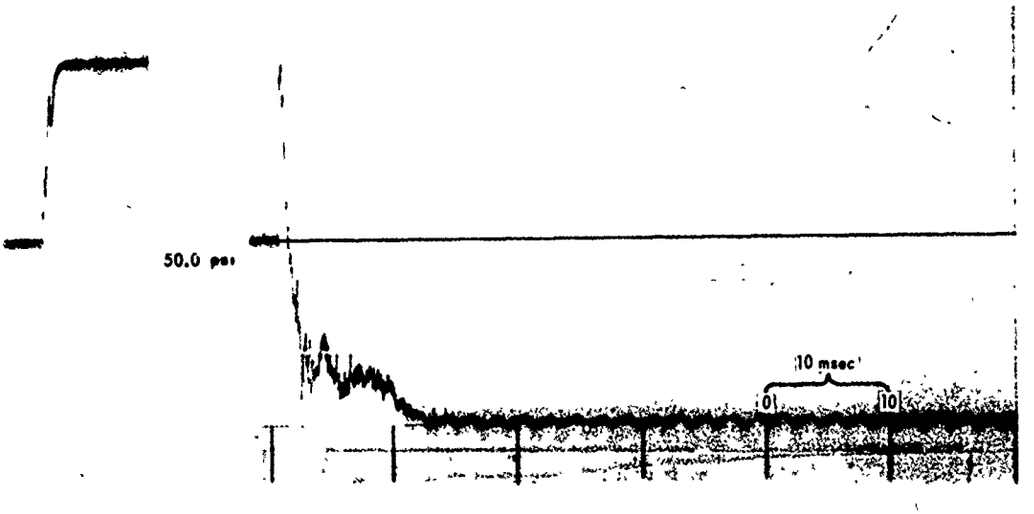

10 O'CLOCK LEG
STATION 5 CALIBRATION STEP AND PRESSURE–TIME SHOCK PROFILE

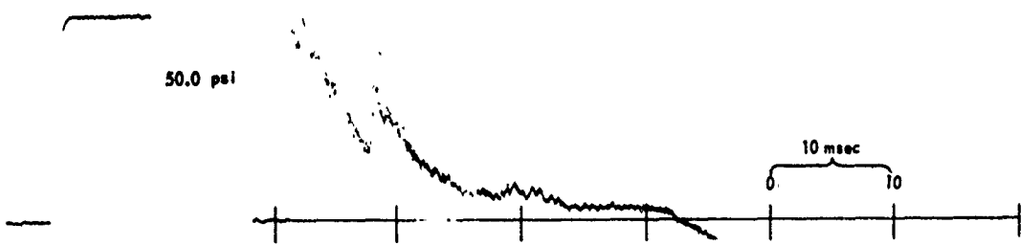

6 O'CLOCK LEG
STATION 5 CALIBRATION STEP AND PRESSURE-TIME SHOCK PROFILE

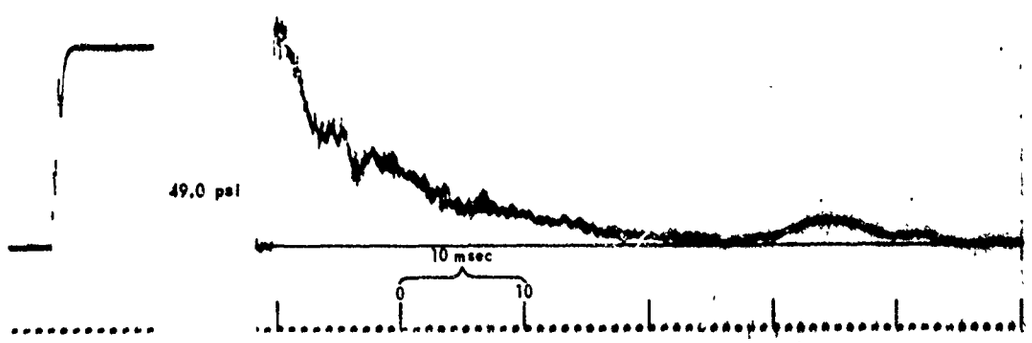

2 O'CLOCK LEG TIME PULSE
STATION 5 CALIBRATION STEP AND PRESSURE-TIME SHOCK PROFILE

Figure 19. Side-On Overpressure, Station 5, Test CD-96.

None

NO GAUGE WAS INSTALLED

10 O'CLOCK LEG
STATION 6 CALIBRATION STEP AND PRESSURE-TIME SHOCK PROFILE

6 O'CLOCK LEG
STATION 6 CALIBRATION STEP AND PRESSURE-TIME SHOCK PROFILE

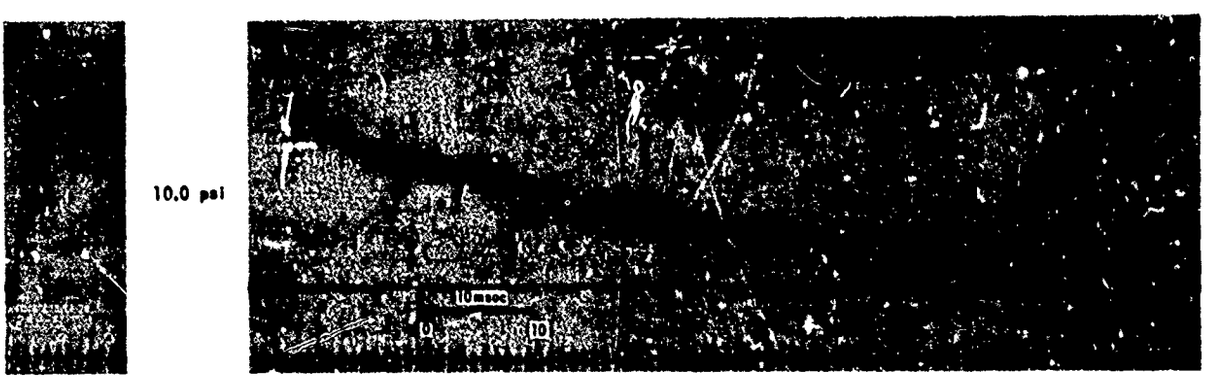

TIME PULSE

2 O'CLOCK LEG
STATION 6 CALIBRATION STEP AND PRESSURE-TIME SHOCK PROFILE

Figure 20. Side-On Overpressure, Station 6, Test CD-96.

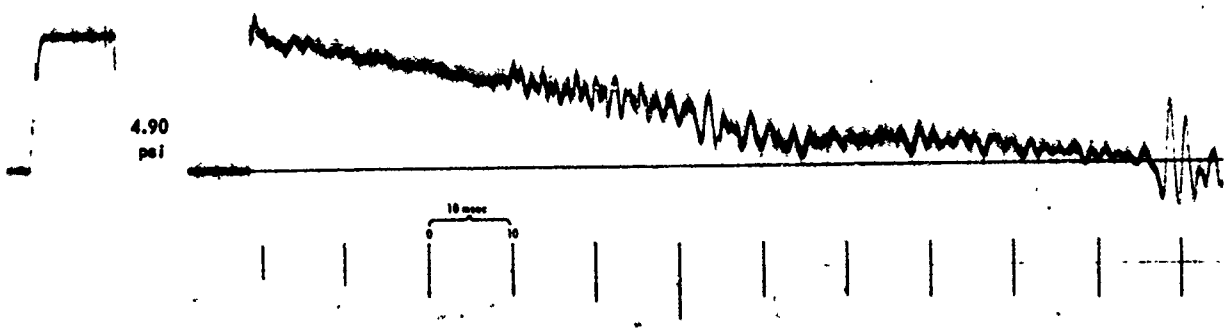

10 O'CLOCK LEG
STATION 7 CALIBRATION STEP AND PRESSURE-TIME SHOCK PROFILE

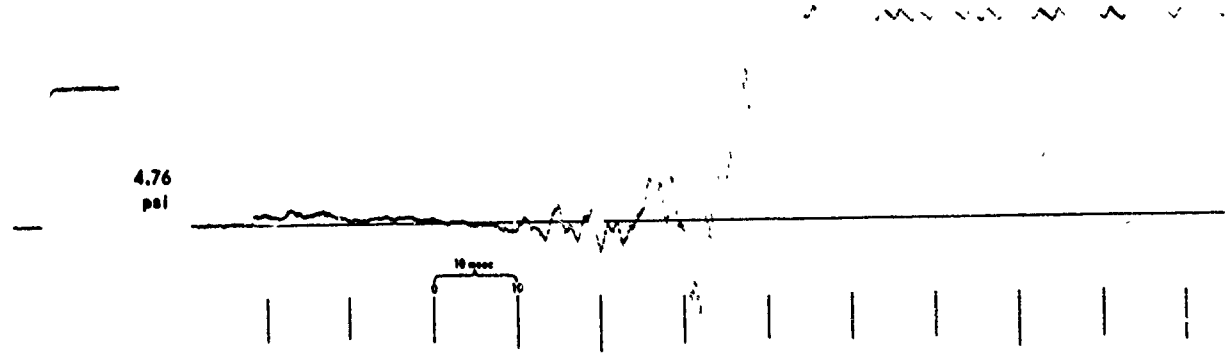

6 O'CLOCK LEG
STATION 7 CALIBRATION STEP AND PRESSURE-TIME SHOCK PROFILE

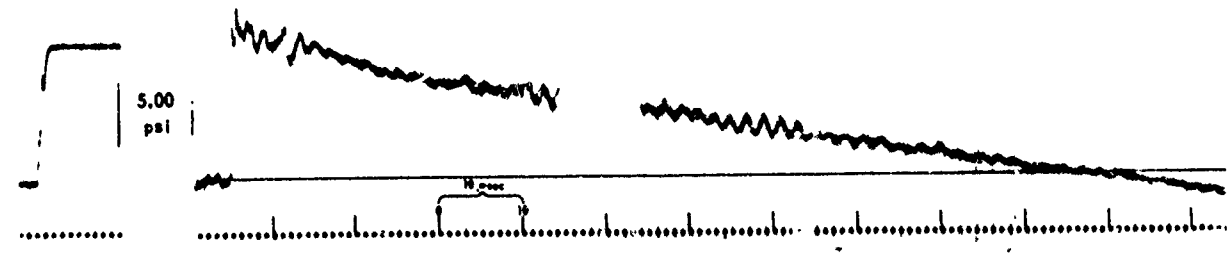

2 O'CLOCK LEG TIME PULSE
STATION 7 CALIBRATION STEP AND PRESSURE-TIME SHOCK PROFILE

Figure 21. Side-On Overpressure, Station 7, Test CD-96.

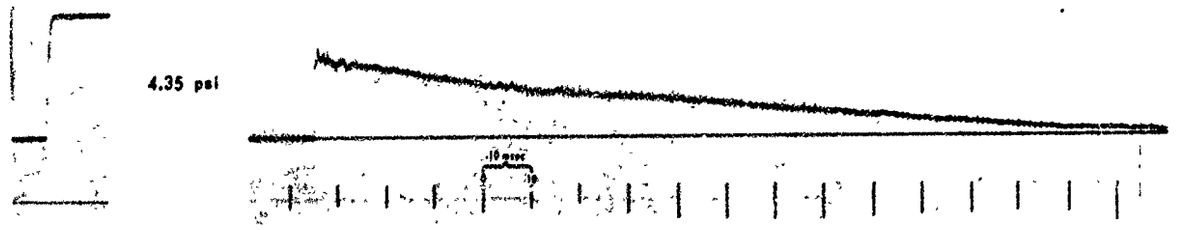

10 O'CLOCK LEG
STATION 8 CALIBRATION STEP AND PRESSURE-TIME SHOCK PROFILE

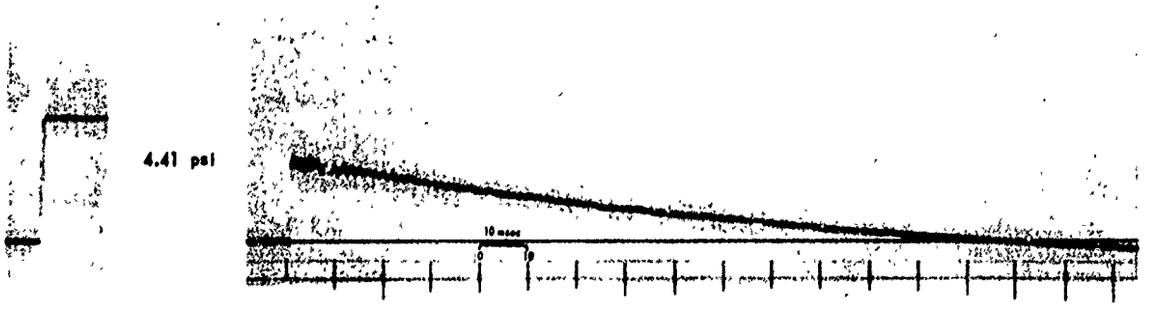

6 O'CLOCK LEG
STATION 8 CALIBRATION STEP AND PRESSURE-TIME SHOCK PROFILE

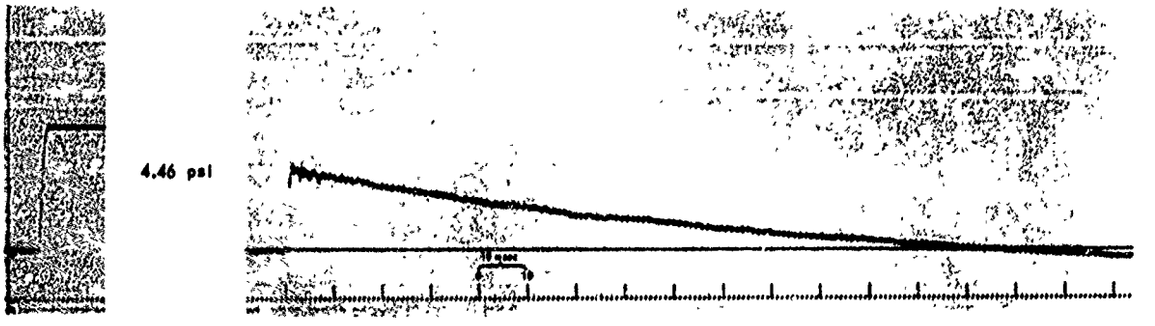

2 O'CLOCK LEG TIME PULSE
STATION 8 CALIBRATION STEP AND PRESSURE-TIME SHOCK PROFILE

Figure 22. Side-On Overpressure, Station 8, Test CD-96.

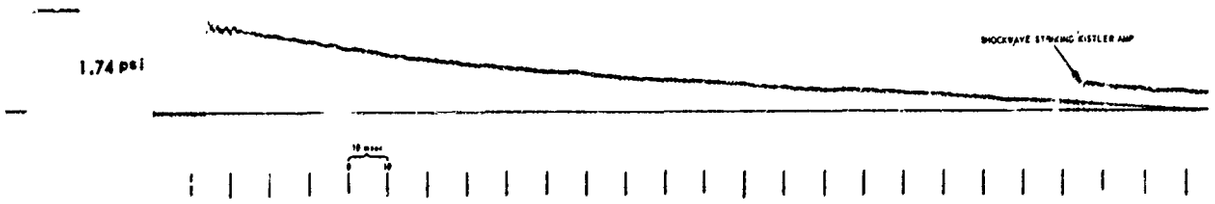

10 O'CLOCK LEG
STATION 9 CALIBRATION STEP AND PRESSURE-TIME SHOCK PROFILE

6 O'CLOCK LEG
STATION 9 CALIBRATION STEP AND PRESSURE-TIME SHOCK PROFILE

2 O'CLOCK LEG
STATION 9 CALIBRATION STEP AND PRESSURE-TIME SHOCK PROFILE

Figure 23. Side-On Overpressure, Station 9, Test CD-96.

6 O'CLOCK LEG
STATION 5 CALIBRATION STEP AND PRESSURE-TIME SHOCK PROFILE

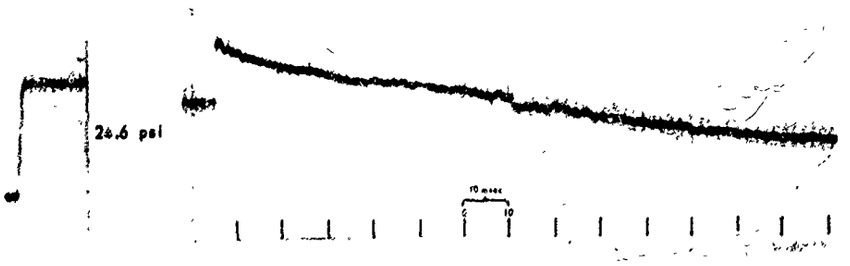

6 O'CLOCK LEG
STATION 6 CALIBRATION STEP AND PRESSURE-TIME SHOCK PROFILE

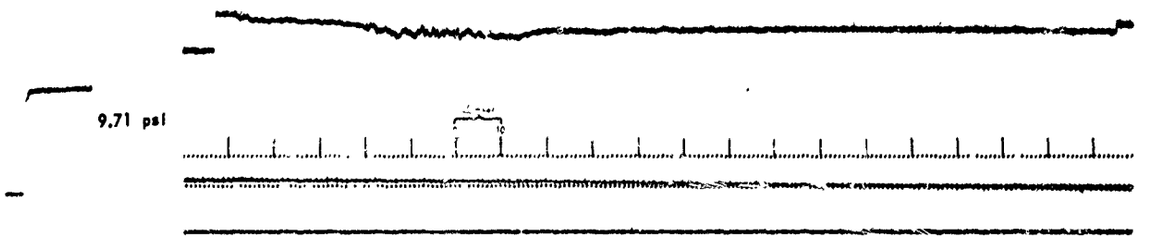

6 O'CLOCK LEG TIME PULSE
STATION 8 CALIBRATION STEP AND PRESSURE-TIME SHOCK PROFILE

Figure 24. Face-On Overpressure, Test CD-96.

Blast overpressures are reported in Table 9 as read from these records, using the calibration steps. The data are preliminary, however, because post test calibration of the Kistler systems has not yet been completed by the Air Force. Loop-gain setting errors in the amplifiers were thought to be as high as 40 percent. Consultation with Aerojet engineers revealed an error in the calibration procedure and subsequent correct calibrations were found to be generally no larger than 3 percent. Although all the amplifiers have been calibrated for their loop-gain error, the Kistler transducers have not yet been subjected to static field calibration. As soon as the field calibration has been completed, appropriate corrections to the data presented in Table 9 will be made. It is anticipated that the over-all correction will be less than 10 percent in all cases.

In Table 9 overpressures and TNT equivalences are calculated by solution of the Rankine-Hugoniot equations using time-of-arrival data obtained at the gauge stations. Since this method is generally applicable to the pressure range of 5 to 90 psi, calculated values are shown only within this range. Also in Table 9 the impulse data and TNT equivalences are based on impulse. Obviously the impulse data is dependent upon the system calibration results and must be considered preliminary data.

4.1.3.4 Radiation Data

The thermal radiation data, gathered by means of radiometers, Deltacouples, and a pyrometer, cannot be reduced. The extremely high level of electromagnetic radiation produced by the detonation detrimentally affected all channels by producing excessive noise in the initial portions of the pulses. The shock wave arrival on the output of the radiometer stations was marked by an abrupt negative sweep. The Deltacouple signals contained extraneous noise and appeared to cross-talk. The Deltacouple records and the system itself were discussed in May with the system's developer to determine methods by which its output may be improved. The pyrometer data are unusually low, probably because the fireball was obscured from the pyrometer by the dust clouds along the surface of the ground. Study of the film records suggests that the pyrometer should be placed farther above ground level in subsequent tests. This change may be required also for the other thermal devices.

Table 9. Side-on Overpressures and Impulses, with TNT Equivalences, Test CD-96.

NOTE: The data in this table are preliminary. Their values are subject to change after further analysis.

Radial Distance from Charge (ft)	Radial Direction (see Fig. 13)	Peak Overpressure†		TNT Equivalence		Measured Impulse (psi-msec)	TNT Equivalence from Measured Impulse (%)
		Measured (psi)	Calculated (psi)	from Measured Overpressure (%)	from Calculated Overpressure (%)		
250	2	54.0	-	223	-	549	101
	6	50.3	-	208	-	430***	57***
	10	*	-	*	-	*	*
375	2	**	20.2	**	193	-	-
	6	**	19.8	**	188	-	-
	10	**	19.5	**	184	-	-
500	2	10.1	-	155	-	334	122
	6	*	-	*	-	*	*
	10	**	-	**	-	**	**
600	2	**	6.81	**	136	-	-
	6	**	6.71	**	131	-	-
	10	**	6.35	**	123	-	-
700	2	5.52	-	177	-	251	131
	6	*	-	*	-	*	*
	10	5.51	-	151	-	224	106
1000	2	2.98	-	132	-	174	127
	6	2.90	-	126	-	180	136
	10	2.95	-	130	-	211	178
1500	2	1.45	-	92	-	139	169
	6	1.73	-	145	-	118	127
	10	1.57	-	115	-	151	192

† Measured overpressures are derived from Kistler transducer measurements. The calculated overpressures are calculated at midpoint distances between Kistler transducer stations from which time-of-arrival data are available. The calculations are performed using an equation derived from the Rankine-Hugoniot equations:

$$p = \frac{2\gamma}{\gamma+1} P_o \left(\frac{U^2}{c_o^2} - 1 \right)$$

where

p = peak overpressure on the shock front

γ = ratio of specific heats for air

P_o = test-site atmospheric pressure

U = velocity of shock front

c_o = sound velocity at test site

* No data, because of gauge failure.

** No side-on overpressure gauge placed at this location.

*** Record difficult to read for impulse determination.

4.2 CONCLUSIONS

This composite propellant in a solid 6-ft-diameter cylindrical configuration definitely will sustain detonation. This affirms the validity of the theoretical and experimental approach used in SOPHY I to determine the approximate region to test for the critical diameter of unadulterated propellant. Beyond this, the results of Test CD-96 show that today's solid propellant is capable of sustaining detonation in sizes that are comparable to the large booster designs presently envisioned, for the critical geometry theory predicts that, without interaction by jetting, the critical web thickness is one-half the critical diameter for circular-core cylinders. The precise factor may differ from "one-half," but the fact remains that detonation over a finite length has been observed with adulterated propellant charges having webs near one half of the critical diameter.

The major question left unanswered is that of sensitivity to initiation. Sensitivity has gained considerable practical importance because of the CD-96 results but it has always been an integral part of the complete SOPHY approach to the study of large solids hazards. Included in Phase II of Task I of this contract are tests designed to investigate and utilize a method by which an estimate of unadulterated propellant sensitivity might be made by testing subcritical samples.

5. PROPELLANT DEFECTS STUDY

Aerojet's Sacramento Plant, Research and Technology Operations (R&TO) will prepare and characterize propellant containing unconnected pores and connected voids. This program will be concerned with developing techniques for studying the effects of physical defects on propellant detonability and sensitivity and on the thermal explosion hazard presented by subcritical samples.

For the investigation, 10 lb and 60 lb batches will be used, the latter for evaluation of the reproducibility of the technique when applied to larger batches and different mixing equipment. Creation of unconnected porosity will be attempted chemically and physically in order to produce porosity of a specific pore-size range. Connected voids will be prepared physically, and the resulting material will be characterized by surface area measurement and other applicable techniques.

Because of manpower considerations, the program could not be initiated by R&TO until the latter half of May. Preparations are being made to launch into the study in June with full time effort.

6. FUTURE PLANS

During the next quarterly period, June through August 1966, the following work will be performed:

a. Completion of Phase I tests.

b. Continuation of Phase II tests.

c. Firing of the 60-in.-diameter and 84-in.-diameter large critical diameter tests.

d. Continuation of propellant defects literature search.

e. Continuation of the preparation and characterization of propellant with defects.

REFERENCES

1. Large Solid-Propellant Boosters Explosive Hazards Study Program (Project SOPHY), Technical Documentary Report AFRPL-TR-65-211, Aerojet Report 0866-01(01)FP (November 1965).

2. Salzman, F.K., O.R. Irwin, and W.H. Andersen, "Theoretical Detonation Characteristics of Solid Composite Propellants," AIAA Journal, Vol. 3, No. 12, pp 2230-2238 (December 1965).

3. Project SOPHY - Solid Propellant Hazards Program, Technical Documentary Report AFRPL-TR-66-24, Aerojet Report 0977-01(02)QP (March 1966).

4. Cachia, G.P., and Whitbread, E.G., "The Initiation of Explosives by Shock," Proc. Royal Soc., A246, 268 (1958).

5. Bowden, F.P., "The Initiation and Growth of Explosion in the Condensed Phase," 9th Symposium on Combustion, 499-516 (1963).

6. Maycock, J.N., and Grabenstein, D.E., "Piezoelectricity in Secondary Explosives," Science, Vol. 152, 508-9 (1966).

7. Adams, G.K., Holden, J., and Whitbread, E.G., "The Explosive Initiation of a Single Crystal of Cyclotrimethylene Trinitramine," Conf. Inter. de Chem. Ind, pp 7-8 (September 1958).

8. The Design and Analysis of Sensitivity Experiments, Rocketdyne Report R-6152 (May 1965).

9. Project SOPHY - Solid Propellant Hazards Program, Aerojet Report 0977-01(01)ER (December 1965).

10. Project SOPHY - Solid Propellant Hazards Program, Aerojet Report 0977-01(02)MP (November 1965).

11. Price, D. Large Scale Gap Tests: Interpretation of Results for Propellants, NOL-323, NAVWEPS 7401, 15 March 1961.

APPENDIX A

COMMENTS ON THE RUBY CODE*

1. INTRODUCTION

The RUBY Code (Reference A-1) is a FORTRAN computer program designed to calculate the ideal detonation properties of high explosives utilizing Chapman-Jouguet (C-J) theory. The program is based on the assumption that the gaseous products obey the Becker-Kistiakowsky-Wilson (BKW) equation of state (References A-2 and A-3), which can be written as

$$\frac{PV}{nRT} = 1 - X \exp(\beta X) \qquad \text{(A-1)}$$

where

$$X = \frac{\kappa \sum_i k_i n_i}{V (T+\theta)^{\alpha} \sum_i n_i}$$

Here, α, β, κ, θ, k_i are constants, and n_i is the mole fraction of the i^{th} gaseous product.

In RUBY, this P, V, T relation is used to express the one-dimension detonation conservation equations and C-J hypothesis (i.e., $D = C_J + W_J$) in terms of P, V, T variables, and also to describe the fugacity of the gaseous reaction products as a function of pressure and temperature. In addition, RUBY employs an equation of state of the form

$$P = \sum_{j=0}^{4} a_j (\rho_s/\rho_{s,o})^j + \sum_{k=0}^{1} b_k (\rho_s/\rho_{s,o})^k T + \sum_{m=0}^{2} c_m (\rho_s/\rho_{s,o})^{-m} T^2 \qquad \text{(A-2)}$$

to handle the possible existence of one or two solid detonation products.

*R. F. Chaiken, Technical Consultant, Aerojet-General Corporation, Downey, California.

The C-J state is assumed to be at thermodynamic equilibrium (minimum free energy) and is calculated by a method of steepest descent, which is described by White, et al (Reference A-4).

The main use of RUBY to date has been in the calculation of ideal detonation properties of CHNO explosives (References A-2, A-3, A-5, A-6)*. The general approach has been to determine the BKW constants (i.e., α, β, κ, θ, k_i) which allow the best fit to the experimental $D(\rho_o)$ and $P_J(\rho_o)$ data for one or two specific explosives (e.g., RDX, PETN), and after selecting these constants, to apply RUBY to other explosives.

Generally, the RUBY calculated $D(\rho_o)$ and $P_J(\rho_o)$ for CHNO explosives are in fair agreement with experiment; however, there is apparently no single set of BKW parameters which yields good agreement with all twenty of the explosives considered. For example, Table 4 in Reference A-5 illustrates that detonation velocities and pressures may be in error by as much as 10% and 15%, respectively. Also, while there is a lack of reliable experimental data on detonation temperatures, it would appear that RUBY values of T_J may be up to 40% too low.

The purpose of this report is to examine the results of the RUBY program and to determine its usefulness in calculating the ideal detonation properties of conventional solid propellants containing ammonium perchlorate, aluminum, and oxygen-deficient rubber-type binders. Of particular interest is the use of RUBY to determine the effect of incomplete chemical reaction on the ideal detonation properties (D, P_J, T_J). Toward this end, RUBY calculations have been carried out for ammonium perchlorate (AP), alone and in combination with typical propellant ingredients, and for RDX/aluminum mixtures. Computer-input techniques were developed to allow various amounts of aluminum to remain unreacted. These calculations brought out certain apparent internal inconsistencies which suggest that RUBY should not be used to predict the detonation properties of aluminized explosives.

*References A-2 and A-3 do not refer to RUBY calculations per se, but to similar calculations using the BKW equation of state.

2. RUBY CALCULATIONS

2.1 AMMONIUM PERCHLORATE

The detonation properties of ammonium perchlorate (AP) have been calculated by RUBY over the range of loading densities $0.8 \leq \rho_o \leq 1.5$ gm/cc. Various sets of BKW constants have been employed to attempt to match the reported experimental data (References A-7 and A-8), as well as to ascertain the sensitivity of the computed detonation properties to changes in the BKW constants.

The results of these calculations are shown in Figures A-1 through A-3 where ideal detonation velocity (D), Chapman-Jouguet pressure (P_J), and Chapman-Jouguet temperature (T_J) are plotted against ρ_o. The notes for Figures A-1 through A-3 describe the conditions for obtaining curves A through F. These results show that by suitable adjustment of the BKW constants (α, β, κ, θ. and in particular, k_i for the principal gas products, e.g.,HCl) almost any linear $D(\rho_o)$ curve can be obtained.

However, the constants that have been derived for best fit with CHNO explosives (e. g., curves A and B), although yielding reasonable agreement with the experimental P_J value at ρ_o = 1. 0 gm/cc, do not yield good agreement with the experimental D value. Even curve E, which is presumably the result of SRI's attempt (Reference A-8) to optimize the BKW constants for AP, falls short of being in good agreement with experimental detonation velocities.

With regard to the RUBY-calculated Chapman-Jouguet temperatures, it is readily seen that an increase in ρ_o results in a decrease in T_J. This $T_J(\rho_o)$ relationship appears to be common to all RUBY calculations, including those for CHNO explosives (References A-2, A-3, A-5, and A-6). This undoubtedly arises from the fact that the BKW equation of state considers only a repulsive potential between the detonation products. On the other hand, curve F, which corresponds to calculations with Cook's covolume equation of state (Reference A-9), shows $T_J(\rho_o)$ to be an increasing function of loading density. Cook's covolume depends only on volume and hence does not consider the potential energy arising from intermolecular interaction. Unfortunately, the present lack of reliable experimental T_J data precludes a clear-cut answer as to whether T_J should be an increasing or decreasing function of ρ_o.

In the case of high-density CHNO explosives, it has been argued (Reference A-2) that since the C-J density (ρ_J) is generally greater than the explosive crystal density, the distances between atomic and molecular species in the C-J plane are so small so that the interactions between the species are primarily repulsive (hence, the BKW-type of equation of state).

In this case, even though the total change in specific internal energy of detonation increases with ρ_o, the net result could be to increase the potential energy of the C-J system at the expense of the kinetic energy.

However, for ammonium perchlorate at the loading densities considered here, ρ_J is less than the crystal density (1.95 gm/cc). It is difficult therefore to understand why the above argument should still be valid under these conditions. It is believed that the RUBY-calculated decrease in T_J as ρ_o increases is unrealistic for AP. On the other hand, it should be stated that the T_J values obtained for AP by use of the Cook-covolume equation of state, which are 600-700°K higher than the AP adiabatic flame temperature (1 atm), might also be unreasonable. However, the increasing $T_J(\rho_o)$ function that is obtained by such a covolume equation of state is, at least to this writer, intuitively plausible.

2.2 SOLID COMPOSITE PROPELLANT

RUBY calculations have been carried out for a solid composite propellant composition containing AP, aluminum, and PBAN binder (polybutadiene-acrylonitrile copolymer). The effect of replacing part of the AP with RDX on the detonation properties has been calculated, as well as the effect of nonreaction of the aluminum. This latter effect corresponds to a current theory that the aluminum oxidation reaction proceeds too slowly to occur within the detonation reaction zone (Reference A-10).

Prevention of aluminum oxidation in the RUBY calculation is readily accomplished by replacing all or part of the aluminum in the explosive composition by the fictitious metal AlX. The AlX has all the thermodynamic properties of Al, but no oxidation products (e.g., AlX_2O_3, $AlXO_2$, $AlXCl_3$, etc.).

The results of the RUBY calculations with the BKW constants and thermal data corresponding to curve C in Figures A-1 through A-3 are shown in Table A-1. The data for Propellant A (normal case, with 100% Al reaction) are comparable to data obtained for high explosives with similar heats of explosion. A comparison of Propellant C (9.2%

Table A-1. Detonation Properties of AP Propellant as Calculated by RUBY.

Propellant A: AP/Al/PBAA = 0.69/0.15/0.16 (100% Al reaction)

B: AP/Al/PBAA = 0.69/0.15/0.16 (5% Al reaction)[a]

C: AP/Al/PBAA/RDX = 0.598/0.15/0.16/0.092 (100% Al reaction)

	Propellant		
DETONATION PROPERTIES	A ρ_o = 1.73	B ρ_o = 1.73	C ρ_o = 1.715
D, mm/μsec	7.14	7.40	7.25
P_J, Kbar	226	206	232
T_J, °K	3198	1091	3217
V_J, cc/mole of gas	12.39	14.41	12.61
ρ_o/ρ_J	0.743	0.783	0.743
$E_J - E_o$, cal/gm HE	401	308	415
BKW parameter	5.71	11.38	5.86
C-J composition, 10^{-3} moles/gm HE			
Total Gases[b,c]	28.85	27.74	28 67
CH_4	5.19	5.69	5.76
CO	4.25	nil	4.70
CO_2	1.65	5.40	1.88
Cl	5.73	nil	4.91
ClO	nil	5.04	nil
H_2	0.19	nil	0.15
H_2O	8.44	8.29	6.95
N_2	2.61	2.83	3.44
NH_3	0.65	0.20	0.69
AlCl	0.14	nil	0.18
$AlCl_3$	nil	0.28	nil
Total Solids[b,c]	2.71	5.28	2.69
Al(l)	---	5.28	---
Al_2O_3(c)	2.71	nil	2.69
C(graphite)	nil	---	nil

(a) Unreacted Al goes to Al(l) as a detonation product.

(b) Only products 10^{-5} moles/gm HE are included.

(c) A dash (-) indicates the product was not programmed.

RDX adulterated propellant) with Propellant A shows that the detonation parameters (E, P_J, T_J, E_J-E_o) all increase when the more energetic RDX ($\Delta Q \approx$ 1300 Kcal/gm) replaces AP ($\Delta Q \approx$ 300 Kcal/gm). These results are to be expected. The effect of replacing aluminum (reactive) with AlX (unreactive), is that P_J, T_J, E_J-E_o decrease as might be expected, but there is a 4% increase in the detonation velocity. This is evident by comparing Propellant A with Propellant B.

Examination of the gaseous detonation products shows that the total amount of gas is the same in the two cases, and that except for an increase in CO_2, with an accompanying decrease in CO, there is little change in gas products when aluminum does not react. From the heats of formation of Al_2O_3, CO, and CO_2, the net enthalpy loss from the explosive system with AlX would be ~850 cal/gm of explosive. It would be difficult to reconcile an increase in detonation velocity with this energy loss. Undoubtedly, the calculated increase in D stems from the value of the BKW parameter (X in Equation A-1), which does change appreciably. Since k_i for CO_2 is 670, vs 390 for CO in these calculations, it is seen that the value of $k \Sigma_i k_i n_i$ in Equation A-1 will increase when CO is converted to CO_2. (When aluminum does not react, there is more oxygen available in the explosive for reaction with carbon. Thus, a greater portion of the carbon is converted to CO_2 than would be the case if aluminum reacted to Al_2O_3.)

When this increase is combined with a decrease in C-J temperature (which results from the AlX not reacting), the BKW parameter becomes excessively large. It is apparent that the accompanying increase in V_J (which results from a lower P_J) is far from enough to prevent the excessively high value of the BKW parameter. The apparent result is an increase in the detonation velocity, which conflicts with the general expectation that D is an increasing function of E_J-E_o for any given explosive. Similar results are obtained for RUBY calculations with RDX/Al mixtures.

2.3 ALUMINIZED EXPLOSIVES

Table A-2 shows the results of RUBY calculations for RDX in combination with Al, AlX, and Al_2O_3 (80/20 mixtures) at the same loading density (ρ_o = 1.94 gm/cc). For additional comparison, the results of a similar calculation for RDX at a slightly different density (ρ_o = 1.8 gm/cc) are also shown. These calculations were carried out with the same set of thermodynamic data and BKW constants. (The set of input data are those obtained from UCRL except for the addition of input data required for the

Table A-2. Detonation Properties of RDX Explosives as Calculated by RUBY.

Explosive A: RDX
B: RDX/Al = 80/20 (100% Al reaction)
C: RDX/AlX = 80/20 (0% Al reaction)(a)
D: RDX/Al_2O_3 = 80/20

DETONATION PROPERTIES	Explosives A	B	C	D
ρ_o, gm/cc	1.80	1.94	1.94	1.94
D, mm/μsec	8.03	8.56	9.11	8.28
P_J, Kbar	287	359	332	297
T_J, °K	1824	3882	2262	2428
V_J, cc/mole of gas	11.71	12.28	11.38	12.05
ρ_o/ρ_J	0.752	0.747	0.794	0.776
$E_J - E_o$, cal/gm HE	472	464	421	410
BKW parameter	9.23	6.86	8.71	8.09
C-J composition, 10^{-3} moles/gm HE				
Total Gases (b, c)	33.80	25.32	27.06	27.21
CH_4	0.38	3.33	0.04	0.36
CO	0.10	4.47	0.17	0.57
CO_2	7.09	2.48	5.45	5.73
H_2	nil	0.04	nil	nil
H_2O	12.72	2.85	10.53	9.57
N_2	13.50	10.38	10.74	10.64
NH_3	0.01	0.83	0.13	0.34
NO	nil	0.05	nil	nil
Al_2O	---	0.91	---	nil
Total Solids (b, c)	5.92	3.31	12.55	6.09
Al(l)	---	---	7.41	---
Al_2O_3 (c)	---	2.80	---	1.96
C (graphite)	5.92	0.51	5.14	4.13

(a) Unreacted Al goes to Al(l) as a detonation product.

(b) Only products > 10^{-5} moles/gm HE are included.

(c) A dash (-) indicates the product was not programmed.

aluminum-containing products: AlO(g), Al_2O(g), Al_2O_2(g), Al(l), and Al_2O_3(c). Presumably, the UCRL data set has been optimized for RDX.)

While a direct comparison of the calculated properties of Explosive A (pure RDX) with Explosive B (20% aluminum) is not possible because the loading densities are not the same in both cases, the addition of reacting aluminum greatly increases the detonation temperature ($\Delta T_J \approx 2000^{\circ}K$). This is further borne out by the drastic drop in T_J when the aluminum is prevented from reacting (Explosive C).

As in the aluminized propellant case, it is readily seen that nonreaction of aluminum (Explosive C) causes an increase in D, while P_J, T_J, and E_J all decrease. Again, the relatively large increase in the BKW parameter with AlX suggests that the conversion of CO to CO_2 may be responsible for this effect.

However, it appears that replacing aluminum by Al_2O_3 (Explosive D) does not show a similar effect, even though in this case Al_2O_3 can be considered as an inert ingredient in the same manner as AlX. A comparison of the detonation products of Explosives C and D does not appear to offer any significant clues to the different effects of the two inert additives on RDX. However, the effective heats of formation used for the two RDX mixtures were somewhat different: 76.8 cal/gm for Explosive C, vs 686 cal/gm for Explosive D. It is suggested that under these circumstances, a direct comparison of the two cases may not be too meaningful without experimental data for both RDX/Al and RDX/Al_2O_3 mixtures.

There are abundant experimental data on aluminized high explosives which show that aluminum lowers the detonation velocity of the pure explosives (Reference 9). It has been proposed that the aluminum either behaves as an inert diluent or that it reacts to Al_2O(g) with an overall endothermic effect. The results of the RUBY code appear to be inconsistent with the experimental results as well as with either of these explanations.

3. DISCUSSION AND CONCLUSIONS

From the RUBY calculations carried out for CHNO explosives and for AP propellants, it is apparent that with sufficient adjustment of the many available parameters in the BKW equation of state, suitable $D(\rho_o)$ and $P(\rho_o)$ data can be calculated for any given explosive. However, it is likewise apparent that the extension of the RUBY calculations, to other explosives with selected BKW constants, may lead to highly questionable results, particularly when those explosives involve new gaseous products. Although this point had already been made clear by Cowan and Fickett in their original paper (Reference A-2), it has apparently not been emphasized by subsequent investigators who have reported RUBY calculations.

In spite of any agreement that one can obtain between RUBY-calculated and experimental detonation velocities and pressures, there are certain internal inconsistencies which throw doubt on the usefulness of the BKW equation of state in calculating detonation properties. These internal inconsistencies involve: (1) a calculated C-J temperature which consistently decreases as ρ_o increases for any given explosive, and (2) the increase in detonation velocity when the aluminum in aluminized explosives does not react to contribute energy to the C-J state. Both of these effects appear to be related to the BKW equation of state which considers the energy of molecular interaction to be solely repulsive. Under the detonation conditions which are normally calculated by RUBY, it is felt that such an equation of state will overemphasize the role of pressure and underemphasize the role of temperature in determining the product distribution and the detonation properties.

In this connection, it is interesting to examine the actual value of the apparent molar covolume (i.e. the excluded volume) that results from the RUBY calculations presented for propellants in Table A-1. By comparing Equation A-1 with a covolume equation of state, i.e.,

$$P(V-b) = nRT \cdot \qquad \text{(A-3)}$$

it can be readily shown that the apparent molar covolume b/n can be expressed as

$$b/n = \frac{RT}{P} X \exp \beta X \qquad \text{(A-4)}$$

For propellants A, B, and C the values of b/n are 11.0, 13.5, and 11.3 cc/mole, respectively. These values represent approximately 90 to 95% of the calculated molar gas volume (V_J), thus indicating an extremely compact C-J state. It seems unlikely that such a state can exist and still be composed of recognizably independent molecular species.

Although the RUBY calculations that have been carried out to date do not exclude the possibility that the noted inconsistencies can be resolved by a complete change in the BKW constants, they do indicate the unsatisfactory nature of the present code with regard to calculating detonation properties of propellants and aluminized explosives. In view of this, and the arguments presented against an equation of state that implies solely repulsive forces, it is suggested that further work with the RUBY code not be continued.

Pending development of a more satisfactory computer program (presumably incorporating a more realistic product equation of state), it is proposed that the Parlin-Andersen-Miller procedure (References A-11 and A-12) used in the SOPHY I program continue to be used to estimate the ideal detonation velocity.

NOTES FOR FIGURES A-1 THROUGH A-3

Curves A and B

RUBY calculations to determine the effect of a change in BKW constants, using the same thermodynamic data:

Curve A: $\alpha = 0.5$; $\beta = 0.09$; $\kappa = 11.85$; $\theta = 400.$

Curve B: $\alpha = 0.5$; $\beta = 0.16$; $\kappa = 10.91$; $\theta = 400.$

The BKW set for Curve A corresponds to the set used by Cowan and Fickett (Reference A-2) for curve-fitting 65/35 RDX/TNT $D(\rho_o)$ data. The BKW set for Curve B corresponds to the set used by Mader (Reference A-3) for curve fitting RDX $D(\rho_o)$ data.

Curves A, C, and D

RUBY calculations to determine the effect of a change in covolume constants using the same BKW constants. Values of k_i for Curves A, C, and D:

	Curve C	Curve D	Curve A
H_2O	360	360	250
H_2	180	180	180
N_2	380	380	380
NH_3	476	476	476
N_2O	670	670	670
NO	386	386	386
O_2	350	350	350
NO_2	670	670	600
HCl	1588	794	643
Cl_2	1157	578	532

Curve A: Covolume set used by SRI in calculating $D(\rho_o)$ for AP (Private communication from L. B. Seeley (January 1966)).

Curve C: Covolume set used by NOTS in calculating propellant detonation properties (Private communication from J. Dieroff (March 1966)).

Curve D: Arbitrary decrease in covolumes of HCl and Cl_2 from those of Curve C.

Curves E and F

Curve E: SRI RUBY calculations, from Reference A-8.

Curve F: AGC calculations, from Reference A-7, using Cook's covolume equation of state fitted to the experimental ideal detonation velocity at ρ_o = 1.0 gm/cc.

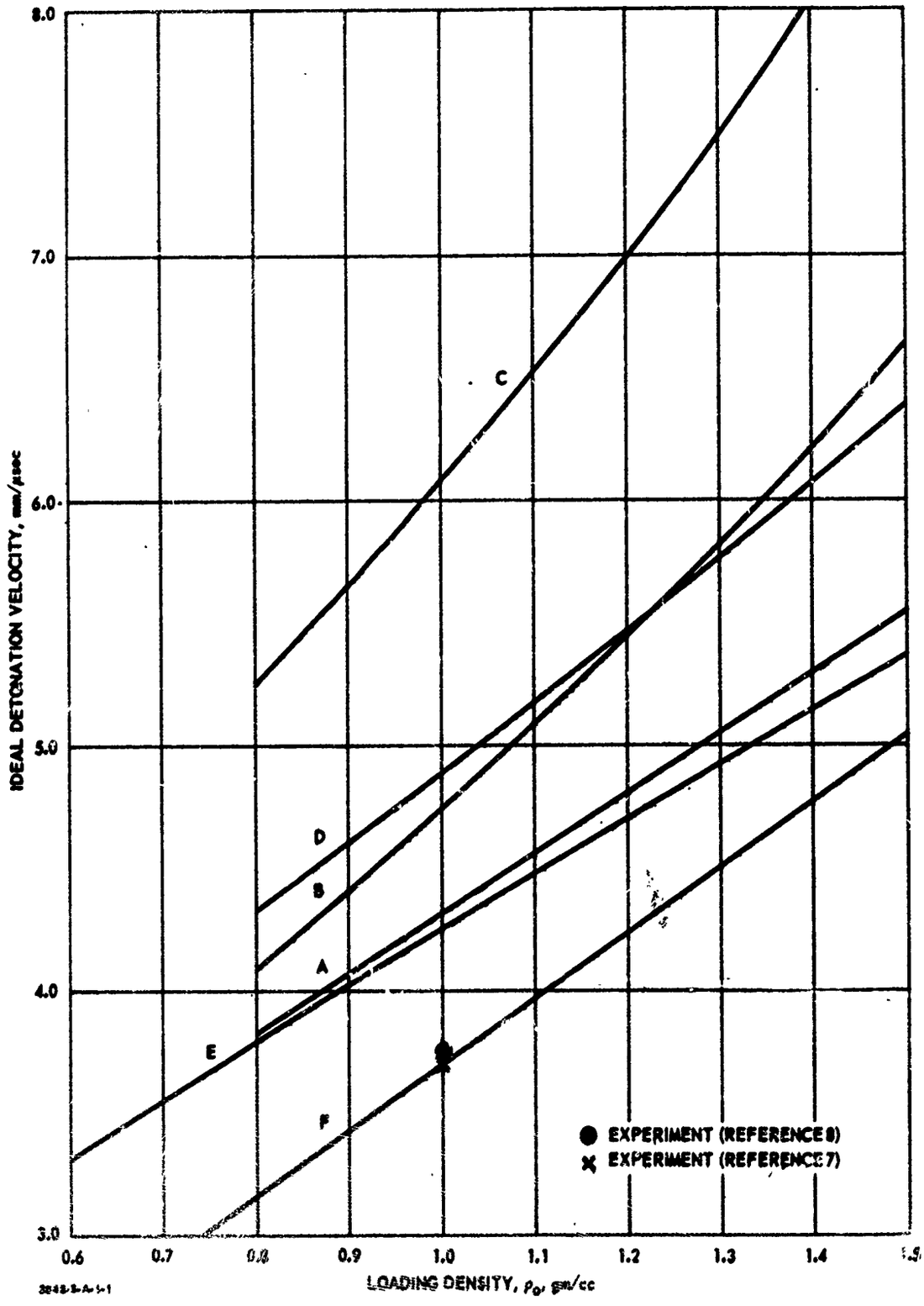

Figure A-1. Calculated Detonation Velocities of Ammonium Perchlorate.

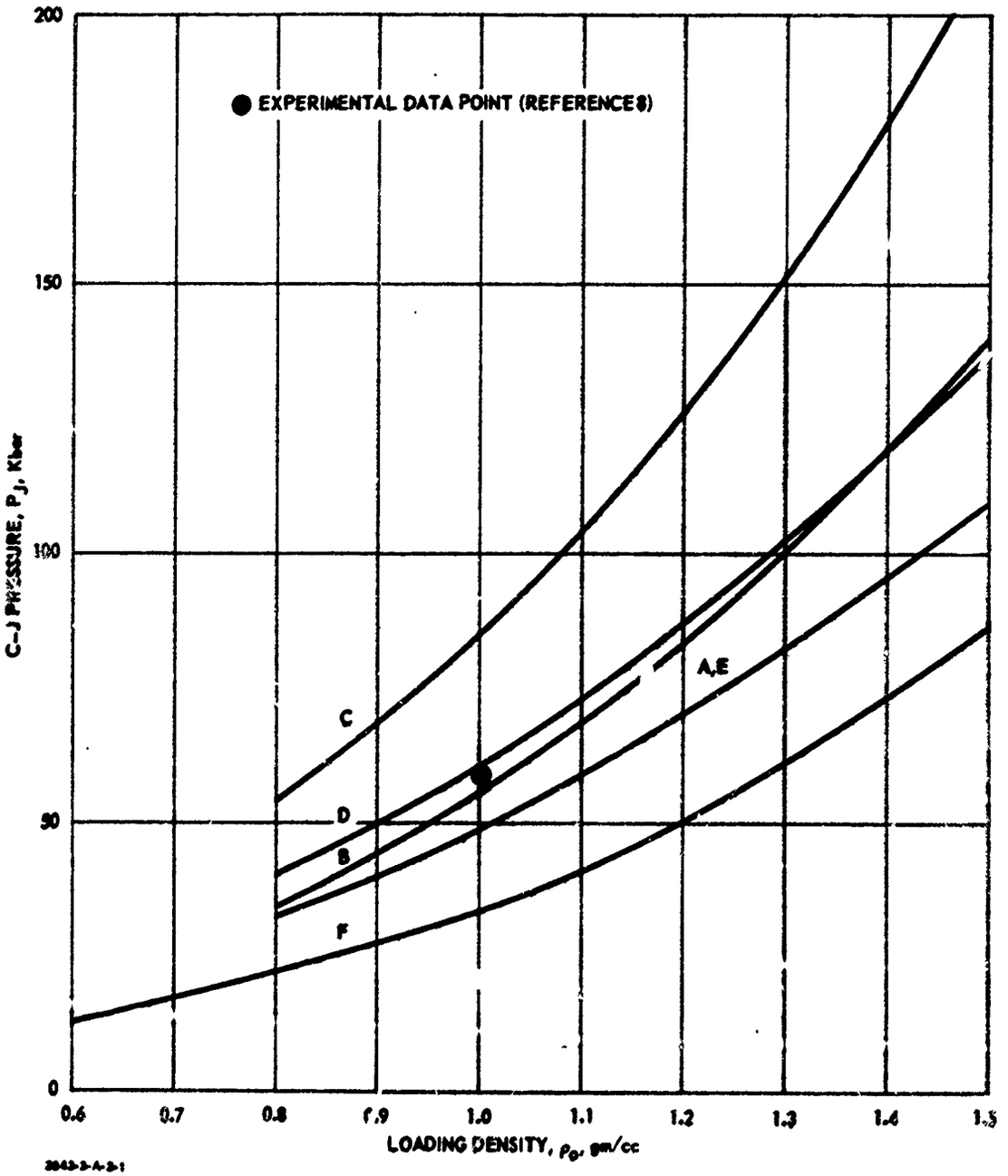

Figure A-2. Calculated Detonation Pressures of Ammonium Perchlorate.

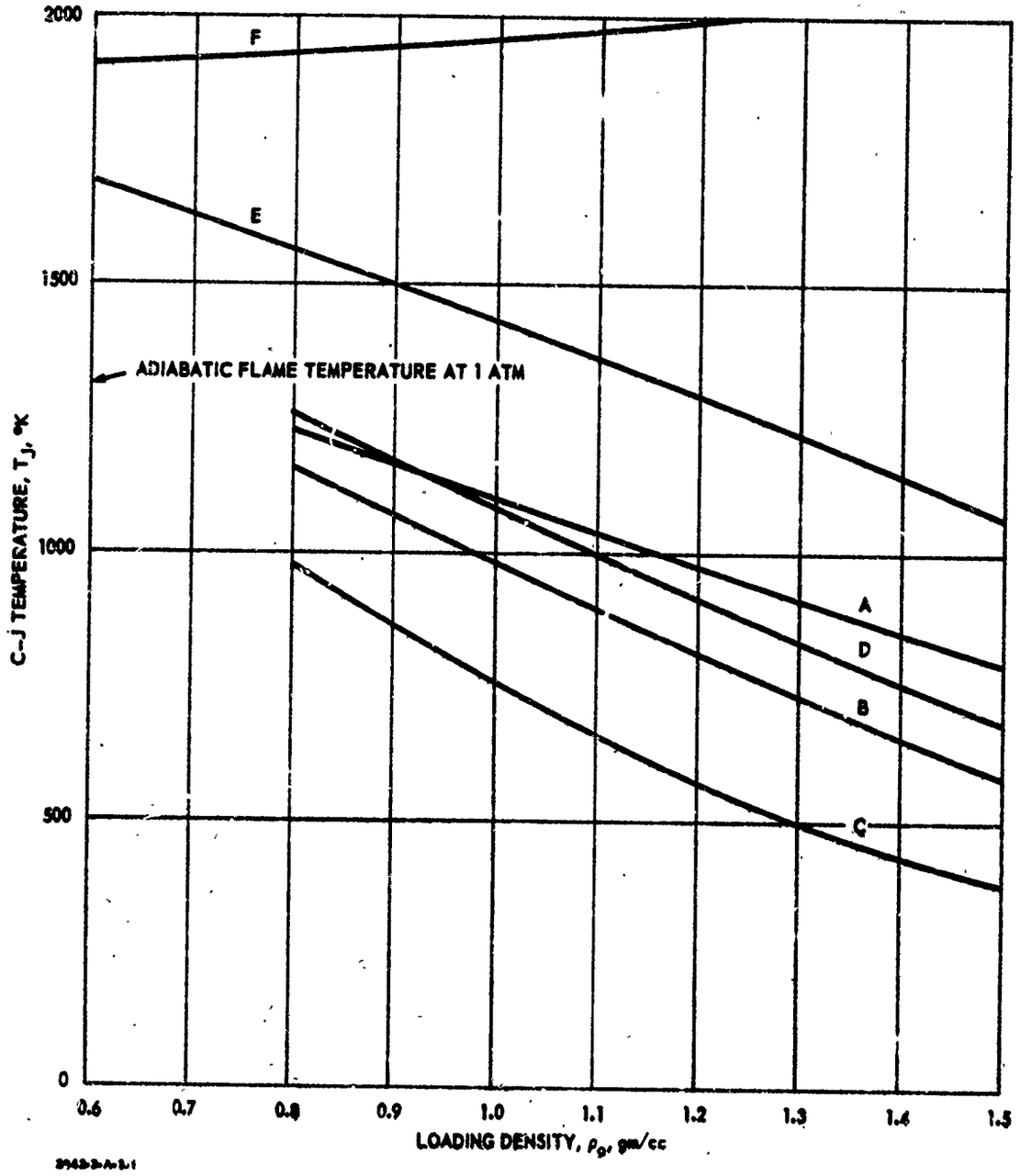

Figure A-3. Calculated Detonation Temperatures of Ammonium Perchlorate.

REFERENCES FOR APPENDIX A

A-1. H. B. Levine and R. E. Sharples, "Operator's Manual for RUBY," UCRL 6815 (March 20, 1962).

A-2. R. D. Cowan and W. Fickett, J. Chem. Phys. 24, 932 (1956).

A-3. C. L. Mader, Los Alamos Report LA-2900 (February 1963).

A-4. W. B. White, S. M. Johnson, and G. B. Dantzig, J. Chem. Phys., 28, 751 (1958).

A-5. D. Price and H. Hurwitz, USNOL, NOLTR 63-216 (1 November 1963).

A-6. H. Hurwitz, USNOL, NOLTR 63-205 (31 March 1965).

A-7. W. H. Andersen and R. E. Pesante, Eighth Symposium (International) on Combustion, Williams & Wilkins Co., Baltimore, Md., p. 705, (1962).

A-8. M. W. Evans, B. O. Reese, and L. B. Seely, The Fourth Symposium on Detonation, Vol. II of Preprints, p. C-78 (12-15 October 1965).

A-9. M. A. Cook, The Science of High Explosives, Reinhold, New York ch. 4, (1958).

A-10. P. K. Salzman, O. R. Irwin, W. H. Andersen, AIAA Journal, 3, 2230, (1965).

A-11. W. H. Andersen and R. B. Parlin, Technical Report No. 28, October 31, 1953, Institute for the Study of Rate Processes, University of Utah.

A-12. R. O. Miller, "Progress in Astonautics and Rocketry: Detonation and Two-Phase Flow," Vol. 6, Academic Press, New York, pp 623-652, (1960).

ACKNOWLEDGEMENT

The writer is indebted to Mr. R. W. Vail, Jr. at Aerojet-General Corporation for his invaluable help in carrying out the RUBY Code calculations presented in this Appendix. The many stimulating discussions held with Dr. O. R. Irwin and Mr. P. K. Salzman are also gratefully acknowledged.

Security Classification

DOCUMENT CONTROL DATA - R&D

(Security classification of title, body of abstract and indexing annotation must be entered when the overall report is classified)

1 ORIGINATING ACTIVITY (Corporate author) Aerojet-General Corporation Downey, California	2a. REPORT SECURITY CLASSIFICATION Unclassified 2b GROUP N/A

3 REPORT TITLE

PROJECT SOPHY - SOLID PROPELLANT HAZARDS PROGRAM

4. DESCRIPTIVE NOTES (Type of report and inclusive dates)

Progress Report, 1 March - 31 May 1966

5. AUTHOR(S) (Last name, first name, initial)

Elwell, R. B.
Irwin, O. R.
Vail, Jr., R. W.

6. REPORT DATE	7a. TOTAL NO. OF PAGES	7b. NO. OF REFS
June 1966	86	10

8a. CONTRACT OR GRANT NO.	9a. ORIGINATOR'S REPORT NUMBER(S)
AF04(611)10919	0977-01(03)QP
b. PROJECT NO. 623A00201	9b. OTHER REPORT NO(S) (Any other numbers that may be assigned this report)
c.	AFRPL-TR-66-25
d.	

10. AVAILABILITY/LIMITATION NOTICES

Qualified requestors may obtain copies of this report from DDC.

11. SUPPLEMENTARY NOTES	12. SPONSORING MILITARY ACTIVITY
	AFRPL, Hazards Analysis Branch AF Systems Command, Edwards AFB Edwards, California

13. ABSTRACT

A final appraisal of the RUBY computer program is presented, which concludes that the program is unsuitable for predicting the detonation properties of typical solid composite propellant. Analysis of the parameter c of the Aerojet detonation model continues. Mean critical diameters of two batches of RDX-adulterated AP-PBAN propellants are compared statistically. The critical-diameter test of a 72-in. dia. sample of unadulterated AP-PBAN propellant resulted in a sustained detonation. The results of the test are presented.

DD FORM 1 JAN 64 1473

Security Classification

Security Classification

14. KEY WORDS	LINK A		LINK B		LINK C	
	ROLE	WT	ROLE	WT	ROLE	WT
Hazards Solid Propellant SOPHY Critical Diameter Critical Geometry						

INSTRUCTIONS

1. ORIGINATING ACTIVITY: Enter the name and address of the contractor, subcontractor, grantee, Department of Defense activity or other organization *(corporate author)* issuing the report.

2a. REPORT SECURITY CLASSIFICATION: Enter the overall security classification of the report. Indicate whether "Restricted Data" is included. Marking is to be in accordance with appropriate security regulations.

2b. GROUP: Automatic downgrading is specified in DoD Directive 5200.10 and Armed Forces Industrial Manual. Enter the group number. Also, when applicable, show that optional markings have been used for Group 3 and Group 4 as authorized.

3. REPORT TITLE: Enter the complete report title in all capital letters. Titles in all cases should be unclassified. If a meaningful title cannot be selected without classification, show title classification in all capitals in parenthesis immediately following the title.

4. DESCRIPTIVE NOTES: If appropriate, enter the type of report, e.g., interim, progress, summary, annual, or final. Give the inclusive dates when a specific reporting period is covered.

5. AUTHOR(S): Enter the name(s) of author(s) as shown on or in the report. Enter last name, first name, middle initial. If military, show rank and branch of service. The name of the principal author is an absolute minimum requirement.

6. REPORT DATE: Enter the date of the report as day, month, year; or month, year. If more than one date appears on the report, use date of publication.

7a. TOTAL NUMBER OF PAGES: The total page count should follow normal pagination procedures, i.e., enter the number of pages containing information.

7b. NUMBER OF REFERENCES: Enter the total number of references cited in the report.

8a. CONTRACT OR GRANT NUMBER: If appropriate, enter the applicable number of the contract or grant under which the report was written.

8b, 8c, & 8d. PROJECT NUMBER: Enter the appropriate military department identification, such as project number, subproject number, system numbers, task number, etc.

9a. ORIGINATOR'S REPORT NUMBER(S): Enter the official report number by which the document will be identified and controlled by the originating activity. This number must be unique to this report.

9b. OTHER REPORT NUMBER(S): If the report has been assigned any other report numbers *(either by the originator or by the sponsor)*, also enter this number(s).

10. AVAILABILITY/LIMITATION NOTICES: Enter any limitations on further dissemination of the report, other than those imposed by security classification, using standard statements such as:

(1) "Qualified requesters may obtain copies of this report from DDC."

(2) "Foreign announcement and dissemination of this report by DDC is not authorized."

(3) "U. S. Government agencies may obtain copies of this report directly from DDC. Other qualified DDC users shall request through _____."

(4) "U. S. military agencies may obtain copies of this report directly from DDC. Other qualified users shall request through _____."

(5) "All distribution of this report is controlled. Qualified DDC users shall request through _____."

If the report has been furnished to the Office of Technical Services, Department of Commerce, for sale to the public, indicate this fact and enter the price, if known.

11. SUPPLEMENTARY NOTES: Use for additional explanatory notes.

12. SPONSORING MILITARY ACTIVITY: Enter the name of the departmental project office or laboratory sponsoring *(paying for)* the research and development. Include address.

13. ABSTRACT: Enter an abstract giving a brief and factual summary of the document indicative of the report, even though it may also appear elsewhere in the body of the technical report. If additional space is required, a continuation sheet shall be attached.

It is highly desirable that the abstract of classified reports be unclassified. Each paragraph of the abstract shall end with an indication of the military security classification of the information in the paragraph, represented as *(TS), (S), (C), or (U)*.

There is no limitation on the length of the abstract. However, the suggested length is from 150 to 225 words.

14. KEY WORDS: Key words are technically meaningful terms or short phrases that characterize a report and may be used as index entries for cataloging the report. Key words must be selected so that no security classification is required. Identifiers, such as equipment model designation, trade name, military project code name, geographic location, may be used as key words but will be followed by an indication of technical context. The assignment of links, rules, and weights is optional.

Security Classification